

Review

Sodium-Ion Batteries: Applications and Properties

Petr Bača , Jiří Libich , Sára Gazdošová and Jaroslav Polkorab

Department of Electrotechnology, Faculty of Electrical Engineering and Communication, Brno University of Technology, Technická 10, 616 00 Brno, Czech Republic; baca@vut.cz (P.B.); 230305@vut.cz (J.P.)

* Correspondence: libich@vutbr.cz

Abstract: With the growing interest in reducing CO₂ emissions to combat climate change, humanity is turning to green or renewable sources of electricity. There are numerous issues associated with the development of these sources. One of the key aspects of renewable energy sources is their problematic controllability, namely the control of energy production over time. Renewable sources are also associated with issues of recycling, utilization in different geographical zones, environmental impact within the required area, and so on. One of the most discussed issues today, however, is the question of efficient use of the energy produced from these sources. There are several different approaches to storing renewable energy, e.g., supercapacitors, flywheels, batteries, PCMs, pumped-storage hydroelectricity, and flow batteries. In the commercial sector, however, mainly due to acquisition costs, these options are narrowed down to only one concept: storing energy using an electrochemical storage device—batteries. Nowadays, lithium-ion batteries (LIBs) are the most widespread battery type. Despite many advantages of LIB technology, the availability of materials needed for the production of these batteries and the associated costs must also be considered. Thus, this battery type is not very ideal for large-scale stationary energy storage applications. Sodium-ion batteries (SIBs) are considered one of the most promising alternatives to LIBs in the field of stationary battery storage, as sodium (Na) is the most abundant alkali metal in the Earth's crust, and the cell manufacturing process of SIBs is similar to that of LIBs. Unfortunately, considering the physical and electrochemical properties of Na, different electrode materials, electrolytes, and so on, are required. SIBs have come a long way since they were discovered. This review discusses the latest developments regarding the materials used in SIB technology.



Academic Editors: Chris Mi, Zhi Cao and Naser Vosoughi Kurdkandi

Received: 16 January 2025

Revised: 30 January 2025

Accepted: 3 February 2025

Published: 6 February 2025

Citation: Bača, P.; Libich, J.; Gazdošová, S.; Polkorab, J.

Sodium-Ion Batteries: Applications and Properties. *Batteries* **2025**, *11*, 61. <https://doi.org/10.3390/batteries11020061>

Copyright: © 2025 by the authors. Licensee MDPI, Basel, Switzerland. This article is an open access article distributed under the terms and conditions of the Creative Commons Attribution (CC BY) license (<https://creativecommons.org/licenses/by/4.0/>).

1. Introduction

The collective effort to reduce greenhouse gas emissions, the replacement of fossil fuels, and the boom in a wide range of different applications, ranging from small portable devices to electric vehicles (EVs) and large stationary off-grid storage, has led to continuous developments in the field of battery storage. In the case of portable devices or, for example, drones, portability and an adequate size and weight are essential. At the same time, safety and cost are of primary importance for stationary storage, where the power output may be in the MW range [1].

Historically, the development of batteries began in about the year 1800 with non-cyclable cells, i.e., primary cells (an illustration of historical development can be seen in Figure 1). As these cells are non-rechargeable with lower energy density, they have been used in low-power consumer electronics. Present-day examples of these cells include,

among others, zinc–carbon cells ($\text{Zn}/\text{MNO}_2+\text{C}$), alkaline cells ($\text{Zn}/\text{MNO}_2+\text{C}$ with KOH electrolyte), silver-oxide cells ($\text{Zn}-\text{Ag}_2\text{O}$) for specific purposes, and lithium batteries (e.g., Li/MnO_2), with an operating life of several years [2,3].

The first battery of the secondary (i.e., rechargeable) type was invented in the middle of the 19th century. It is the lead/acid (Pb/acid) battery and it was invented by Gaston Planté [2]. Since then, the battery has undergone considerable development and its performance has been enhanced. Currently, Pb/acid batteries can reach an energy density of around 30 to 50 Wh/kg at a nominal voltage of 2.1 V. Their application in stationary renewable energy sources, however, is cost-ineffective and not environmentally friendly in terms of their capacity, size, life time, and lead content. Despite these drawbacks, this type of battery is widely used in the automotive industry. At the end of the 19th century, the nickel–cadmium (Ni-Cd) battery was invented as another secondary battery type and a potential competitor to Pb/acid . This battery achieves an energy density ranging from 50 to 75 Wh/kg, has a long life span, and has low self-discharge. However, due to disadvantages such as expensive processing and Cd storage, these batteries did not enter the commercial sphere until the mid-20th century. With respect to their environmental and safety properties, they contain highly toxic Cd and for this reason are subject to regulations in certain countries [2,4]. As a promising successor to Ni-Cd, nickel–metal hydride (Ni-MH) batteries were invented around 1975. This type of battery has a higher energy density in the range of 40 to 110 Wh/kg but has a lower cycling capacity in comparison to Ni-Cd [5].

Since SONY introduced the first LIB battery to the market in 1991, the share of Ni-MH has been on a decline. LIB research itself started in the 1970s to 1980s, and it was at this time that the first SIB research also appeared. However, more research on SIBs followed only in later years, due to the superior properties of Lithium (Li). LIBs have conquered the market of secondary cells due to their high capacity, energy density, nominal voltage, the possibility of faster charging, large operating temperature range, lifespan and nearly absent memory effect [6]. Their capacity has steadily increased over the years and now exceeds 200 Wh/kg and have become the most widespread energy storage devices in terms of installed capacity [7]. The main drawbacks of LIBs today are the Li content itself and, in the case of positive-electrode materials, the presence of cobalt (Co) [3–5,8]. Both of these materials have a very limited supply in the Earth’s crust (Li availability is negligible compared to Na, which makes up 2.36% of the Earth’s continental crust), and their extraction is associated with the unethical treatment of workers [1].

SIB batteries are seen as a possible replacement for LIBs. The properties of Na are very similar to those of Li, and its abundance in the Earth’s crust is a significant advantage (as of 19 November 2024, sodium price is 15 times lower than that of lithium) [9,10]. Sodium mining is not nearly as environmentally demanding, and therefore, sodium appears to be an ideal competitor to lithium. The possibility of using current collectors made of more cost-effective aluminum is another practical advantage of SIBs. Unlike Li, Na does not form alloys with aluminum, so there is no need to use more expensive copper on the negative collector, as is the case with LIBs. This leads to a decrease in the overall battery production cost, as the price of copper is now at USD 9.1 per 1 kg, while a kilogram of aluminum now comes to USD 2.5 [11,12]. However, the different properties of Na come into play when it comes to the use of both positive- and negative-electrode materials. One of the most significant obstacles is the size of the Na ion (0.102 nm), which is 1.3 times larger compared to the Li-ion (0.076 nm). The dimensions of Na prevent the use of already known materials used for LIBs. For instance, when using a negative graphite electrode with a positive LiCoO_2 electrode, intercalation of Li ions into graphite occurs during discharge, forming Li_xC_6 with a final energy density of about 110 Wh/kg (first LIB) [3]. In 1988, it was found that unlike Li ions, Na ions are not capable of effectively forming intercalating

compounds with graphite. Thus, when the Li ions are substituted by Na ions, they do not form Na_xC_6 , as this bond is unstable. NaC_{64} is formed instead, resulting in a reduction in the theoretical capacity to 35 mAh/g [13]. Using P2- $\text{Na}_{0.7}\text{CoO}_2$ and graphite as electrodes, Hasa et al. obtained an energy density of only 60 Wh/kg [14]. Another disadvantage is the size of the electrodes. Since Na ions are larger, more electrode material is needed in order to achieve the same capacity as in LIBs. As for the nominal voltage, it is lower in SIBs than in LIBs. This is due to the higher electrochemical potential of sodium (-2.71 V vs. Standard Hydrogen electrode, SHE) compared to lithium (-3.04 vs. SHE) [5,8,11–13,15,16]. When compared to LIBs, SIBs do not exhibit as high specific energy densities (Wh/kg) due to factors such as the sloped voltage profiles of layered oxide electrodes and narrow voltage windows of organic electrolytes, and due to different ion sizes [17,18].

The failure of graphite led to the development of alloying (materials forming an alloy with an alkali metal) and conversion (based on an anionic reaction between a transition metal and an alkali metal) materials until 2001 when the group of Dahn et al. demonstrated hard carbon and its properties. By combining Na with a hard-carbon electrode, a reversible capacity of up to 300 mAh/g can be achieved [19]. Since 2010, carbon-based materials have been the subject of increased interest in the field of research. Their simple manufacturing process and high theoretical capacity (up to 500 mAh/g) have been the subject of many studies to date [20,21].

In 2011, Johnson et al. demonstrated the use of amorphous TiO_2 nanotubes as a negative-electrode material for SIBs, with a theoretical capacity of 150 mAh/g. Sodium titanate $\text{Na}_2\text{Ti}_3\text{O}_7$, with a theoretical capacity of up to 200 mAh/g, was introduced by Tarascon et al. in that same year [22,23]. In 2012, the utilization of elements such as tin (Sn) and antimony (Sb) to form alloys in negative electrodes was reported. In the case of Sn, a theoretical capacity of 847 mAh/g can be achieved with the formation of the compound $\text{Na}_{15}\text{Sn}_4$; in the case of Sb, a value of 660 mAh/g can be reached with the formation of Na_3Sb [20,24,25]. During the same year, Kim and Park et al. presented a red phosphorus/carbon composite material with a reversible capacity of 1540 mAh/g in the formation of the Na_3P phase at a ca. 1C rate [26].

In 2014, the negative-electrode material $\alpha\text{-MoO}_3$ was discovered by the group of Hariharan et al. The rocking chair $\text{MoO}_3/\text{Na}_3\text{V}_2(\text{PO}_4)_3$ cell exhibited a plateau voltage of 1.4 V and discharge capacity of 164 mAh/g depending on the weight of the negative electrode [26].

In addition, in 2014, the MXene (transition metal-based carbide, carboxide materials—2D-nanometer layers) material Ti_3C_2 with a reversible capacity of ~100 mAh/g was experimentally developed by the group of Kent and Gogotsi et al. [27]. In 2018, an LSG (laser-scribed graphene) material was discovered by the group of Alshareef et al. with a layer width of 3.8 nm in a 002 lattice arrangement, exhibiting high capacitances of up to 425 mAh/g [28].

There has been a steady increase in the number of published research studies on SIBs over the last decade, as depicted in Figure 2. China is the leading country in terms of the number of contributions in the materials field. A comparison of the number of publications over time and the subsequent distribution by individual countries can be seen in Figure 3.

In recent years, in the field of SIB material science, hard carbon-based materials have been the most promising negative-electrode materials thanks to their satisfactory electrochemical properties. In the context of positive-electrode materials, the trends point towards Prussian blue analogs or transition metal oxides (characterized by non-toxicity, long life/cyclability, safety, etc.). In terms of future SIB development, for example, low-temperature Na-S and Na-O (still rather theoretical) batteries are being discussed [29].

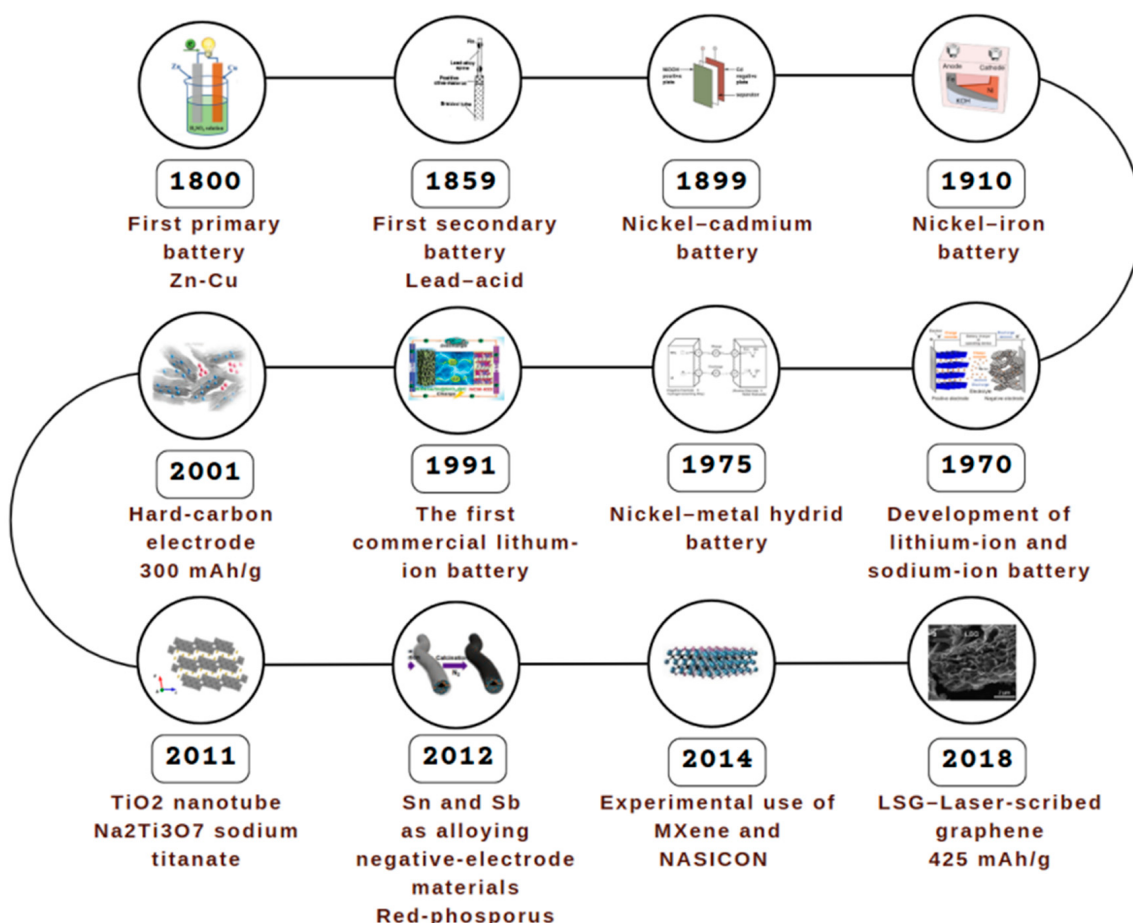


Figure 1. Brief history of battery development [2,28,30–35]. Parts of this figure were adapted with permission from [15,36,37]. Copyright 2020, 2014, 2015 American Chemical Society.

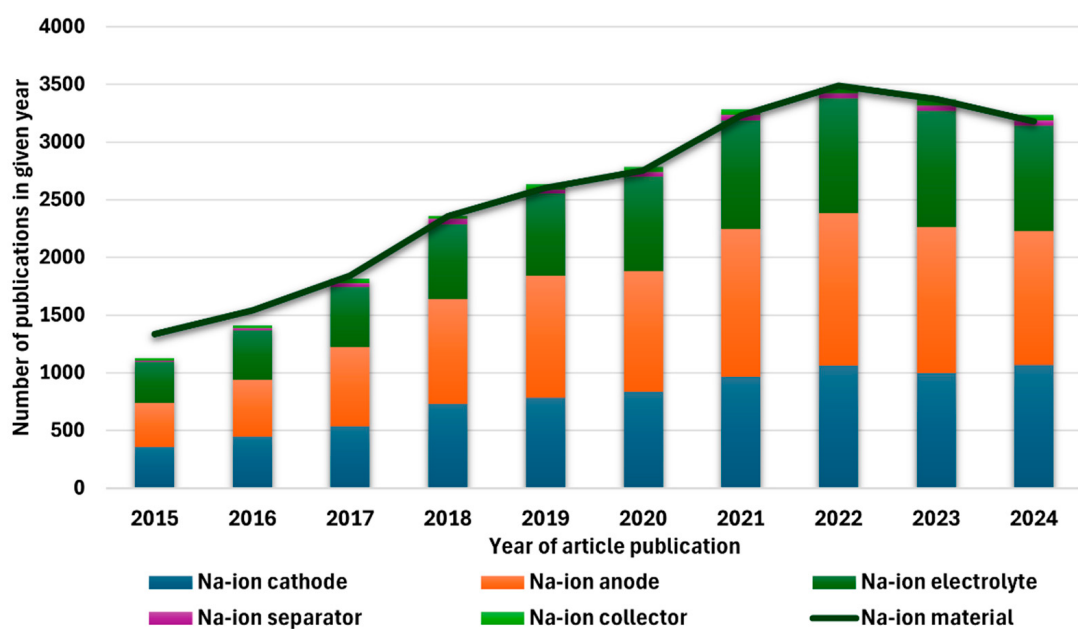


Figure 2. Number of article publications since 2015 according to Web of Science.

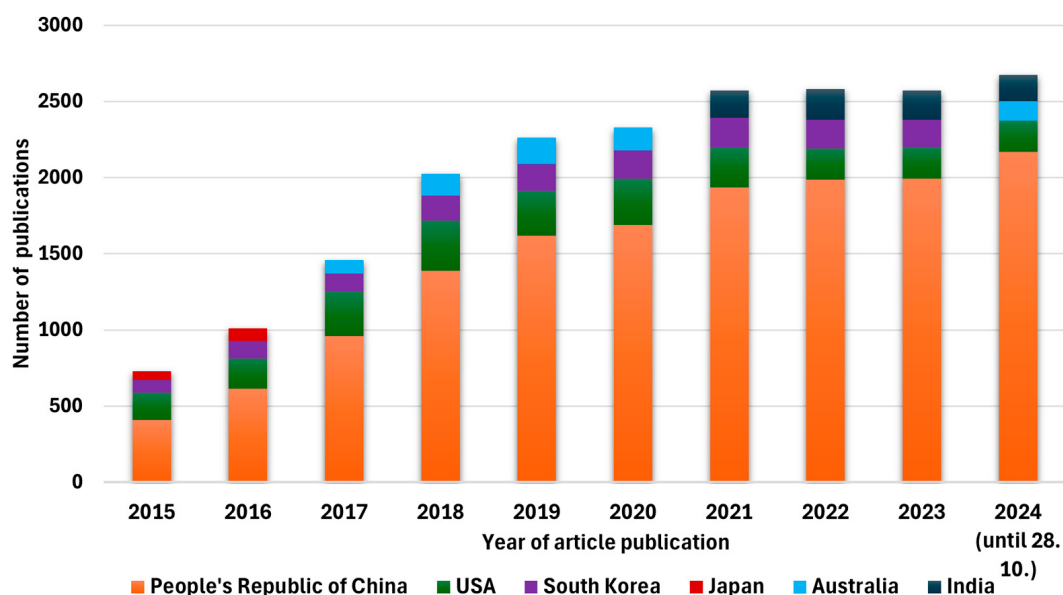


Figure 3. Number of released articles by leading country in each year according to Web of Science.

2. Sodium-Ion Battery Types and Operation Principles

Each part of the SIB cell plays a crucial role in the overall battery performance as the materials directly impact the battery's energy density, safety, lifespan, cost, and much more. The basic cell consists of a positive electrode and a negative electrode, an electrolyte, a separator, and current collectors, which can be seen in Figure 4. SIBs operate on a similar fundamental principle to LIBs, meaning they rely on the reversible movement of ions between the positive and the negative electrodes to either store or release energy. The main difference is that instead of Li ions, Na ions are used as the charge carriers [29]. During the discharge process, sodium ions at the negative electrode release an electron, making them carry a positive charge (Na^+). The Na^+ ions are then transferred to the positive electrode through the electrolyte. In the meantime, the released electrons travel through a current collector and an external circuit, creating a current capable of powering devices. During the charge, an external voltage is applied, forcing the electrons in the positive electrode to flow in the opposite direction toward the negative electrode through the external circuit. At the same time, the Na^+ ions travel through the electrolyte back to the negative electrode, and recombination with the electrons occurs [38].

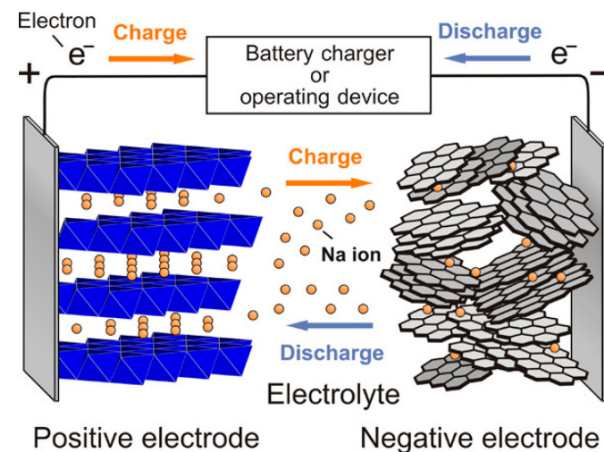


Figure 4. Principle of the sodium-ion battery. Adapted with permission from [15]. Copyright 2014 American Chemical Society.

2.1. Room-Temperature Batteries

According to their ideal operating temperature, batteries can be classified as room-temperature (RT), intermediate-temperature (IT), and high-temperature (HT). Each of these types has its specific properties related to the materials used, the cell construction, and the working principle. The research on SIBs primarily focuses on room-temperature applications due to their similar mechanism to that of LIBs [29].

This review has its main focus on RT SIB and the most used conventional materials and their combinations, which are discussed in more detail in Chapter 3. Among the SIBs capable of operating at room temperature are batteries using sodium metal negative electrodes. The usage of sodium metal as a negative-electrode materials is attractive thanks to their abundance of sodium, high theoretical specific capacity of 1166 mAh/g, and low redox potential. Their biggest limitation is their significant volume change while cycling, leading to the unstable formation of solid electrolyte interphase (SEI) and uncontrollable formation and growth of dendrites. Another disadvantage is the loss of active material due to the presence of an irreversible reaction, which leads to fast capacity fading. These shortcomings become even more serious when paired with a high-capacity sulfur (S) or oxygen (O) positive electrode. Stabilizing the SEI using chemical and physical methods is desirable for constructing a stable sodium metal negative-electrode SIB. A few strategies aiming to overcome this problem have arisen in recent times, such as the utilization of artificial SEI layers, modification of the electrolyte composition (salts, additives, solvents), or usage of 3D current collectors (e.g., copper nanowires) to promote a more homogenous distribution of sodium ions [39].

Na/O₂ batteries as well as Na/S batteries use sodium metal as the negative-electrode material. Na/O₂ is usually made with a liquid electrolyte (usually alkali metal salts in solvents) while using an external O₂ electrode. On the battery casing, openings allow air diffusion on the positive-electrode side, which is also occupied by a porous carbon matrix gas diffusion layer. Na/S batteries are similar to Na/O₂ batteries; however, they are sealed and make use of sulfur hosted in the porous structure of carbon in the positive electrode. The cell configurations can be seen in Figure 5. The role of carbon in this case is to accommodate the large volumetric changes in sulfur during cycling, but also to improve electron conductivity. Both Na/O₂ and Na/S batteries have the potential for fairly high energy densities; however, their development is in the early stages, and even though a great deal of research has been performed on these battery types, they are not yet commercially feasible [38].

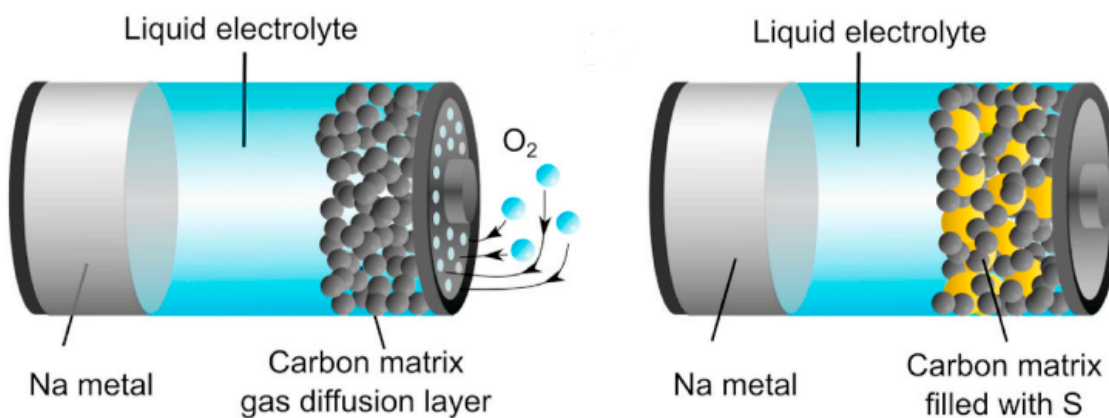


Figure 5. Schematic cell configuration of Na/O₂ and Na/S batteries [38].

2.2. High-Temperature Batteries

Na/S batteries, for example, can operate at high temperatures (typically 300 °C), in which case, both the sodium negative electrode and sulfur positive electrode are in a molten state. In this state, the materials possess high chemical reactivity as well as corrosivity. As these attributes cause serious safety hazards, inert current collectors, stable solid-state electrolytes, and proper sealing need to be used, which ultimately increases the costs of the battery [29,40]. The high reactivity and ion conductivity of molten sodium allow for high current densities (ca. 2.1×10^7 S/m) [41]. Due to high working temperatures, inorganic solid electrolytes (ISEs) are frequently employed, among which an inflexible ceramic material $\beta''\text{-Al}_2\text{O}_3$ (beta alumina) is included [40]. HT Na/S batteries have a life expectancy of over 10 years and have been implemented as test units for stationary energy storage and part of wind and solar installations in, for instance, Japan and the United States [42]. For transportation and stationary energy storage applications, Na/S batteries with organic-based electrolytes seem to be a more suitable option in terms of safety, manufacturing costs, and energy density [40].

MXene materials, such as $\text{Ti}_3\text{C}_2\text{T}_x$, have the potential to be used in elevated temperature conditions. Seredych et al. evaluated the thermal stability of this material, synthesized by selectively etching Al layers from the Ti_3AlC_2 MAX phase. The obtained $\text{Ti}_3\text{C}_2\text{T}_x$ remained stable until 800 °C, at which point it started to degrade, release CO, and transform into cubic titanium carbide (TiC). They also found that a lower concentration of hydrofluoric acid in the etching agent improves the material's thermal stability. Its thermal stability makes $\text{Ti}_3\text{C}_2\text{T}_x$ a promising material for various applications, such as ceramic and matrix composites requiring high-temperature processing [43].

3. Materials for Sodium-Ion Batteries

Specific capacity, cycling stability, and operation voltage are all crucial characteristics of a battery. Among the most important characteristics of the battery is its safety, mainly the thermal runaway issue. Unlike in LIBs, the Al current collectors in NIBs do not undergo dissolution at 0 V; therefore, no short-circuit-causing dendrites are formed, which allows safer storage. However, when discharged to 0 V, SEI in NIBs tends to dissolve and form a thicker layer when charged again, which can lead to sodium metal plating and rollover cell failure [44]. The battery characteristics are all determined by the intrinsic electrochemical properties of the electrode materials, which is why finding suitable electrode materials is essential [29].

3.1. Negative-Electrode Materials

Negative-electrode materials for SIBs can be categorized by the mechanism by which they store sodium ions. These are materials based on intercalation mechanisms, alloying reactions, and conversion reactions. Intercalation-based (also known as insertion-based) materials allow sodium ions to be repeatedly inserted into their crystal structure with minimal structural change. An example of such material is hard carbon, or titanium-based oxides, such as $\text{Na}_2\text{Ti}_3\text{O}_7$. Materials based on alloying reactions work on the principle of forming alloys with sodium during the charging process. These materials provide high theoretical capacities (at the cost of high volume changes) and include tin (Sn), antimony (Sb), silicon (Si), bismuth (Bi), and others [38]. Conversion-type materials undergo chemical conversion reactions during cycling between transition metal oxides (TMOs = Cu, Fe, Mn, Ti...) and alkali metals (Li, Na, K...) using anions (P, O, S, N). TMs include transition metal oxides, transition metal sulfides, transition metal nitrides, and transition metal phosphides. Various storage mechanisms of Na^+ are shown in Figure 6. Similarly to alloying materials, they offer high theoretical capacity with the disadvantage of large volume changes. Another

drawback is the presence of voltage hysteresis, i.e., large voltage differences between charging and discharging, which harms the battery's overall efficiency [45–47].

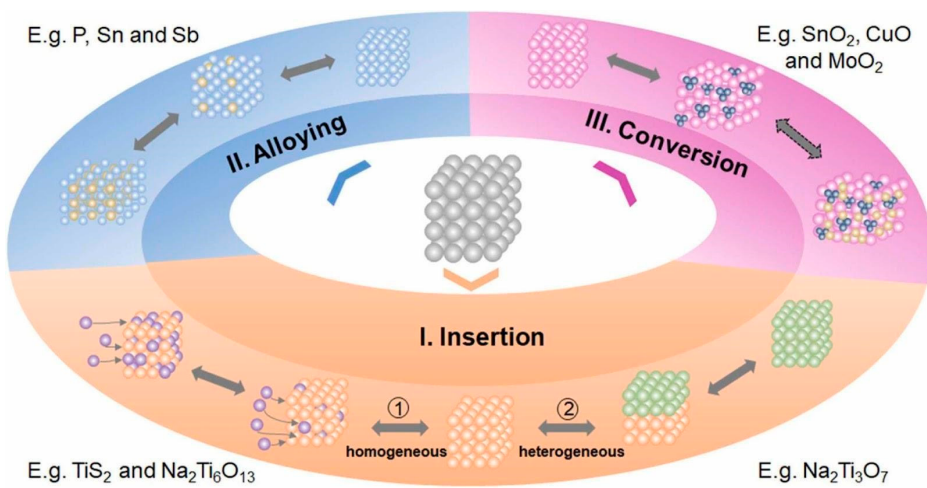


Figure 6. Na^+ storage mechanisms [48].

3.1.1. Insertion Materials

Hard carbon

Hard carbon and its modifications have recently been one of the most researched materials in the negative SIB and LIB electrode fields. Its high reversible capacity of up to 700 mAh/g (with certain modifications), simple production process, and availability make hard carbon a suitable candidate for SIBs [49]. Its development in recent years has mainly focused on biomass processing using the pyrolytic method. The pyrolysis method relies on heating the biomass precursor to temperatures of up to 1000 °C with no air access, which leads to the release of molecules such as H_2O and CO_2 from the material. This release results in high porosity (Brunauer–Emmett–Teller (BET) surface area increase) and surface inhomogeneity, resulting in low ICE (Initial Coulombic Efficiency) and significant loss of active material during SEI layer formation. A gradual increase in temperature beyond 1000 °C leads to material carbonization [50,51]. During carbonization, more stable molecules such as H_2 “evaporate” and form graphene nanodomains, which increase the number of closed HC pores, contributing to increased capacity. For increased hard-carbon purity, HCl, for example, can be used to remove inorganic compounds such as alkali salts or transition metals [52].

Wang et al. used this method in the formation of a negative electrode made from walnut shells, in which the sample carbonized after HCl treatment and firing at 1400 °C showed better electrochemical properties compared to the untreated sample—namely a reversible capacity of 342 mAh/g with a capacity retention of 91% after 100 cycles at a current density of 20 mA/g. This represents simple hard-carbon synthesis with high cyclability. Unfortunately, the use of HCl may be a disadvantage from an environmental point of view. As far as the electrochemical properties are concerned, a high decrease in reversible capacity at higher current densities can be observed, which could affect the utilization of this material in fast-charging batteries [53].

In addition, Kamiyama et al. created a hard-carbon material with MgO nanotubes using the freeze-dry synthesis of magnesium gluconate and glucose. This material shows a reversible capacity of up to 478 mAh/g (depending on the material ratios and firing method) at a current density of 25 mA/g with an ICE of 88% and a reversible capacity of 400 mAh/g at 250 mA/g [54].

In 2022, Zhou et al. created a rosewood-based material. With a specific chemical treatment, the material achieves a reversible capacity of 326 mAh/g at 20 mA/g. The material has the advantage of a reversible capacity of 230 mAh/g at 5000 mA/g. Moreover, it retains 85% of its capacity after 800 cycles at a current density of 500 mA/g [55]. Since these materials are relatively new, more extensive research is required in the future.

In order to mitigate the low ICE typical for hard carbon (typically around 60%), presodation of the negative-electrode material may be used. Chemical presodation, involving the immersion of hard carbon in ether solvents or reductive reagents, seems to provide the best compatibility with the existing SIB manufacturing process. Man et al. were able to improve the ICE of hard carbon by nearly 34% by using tetraethylene glycol dimethyl ether (TEGDME) presodation solution. After pairing the presodiated hard carbon with $\text{Na}_3\text{V}_2(\text{PO}_4)_3$, an ICE of 91.25% was achieved [56].

In the commercial sphere, Faradion Limited uses its own patented hard carbon, which has a specific capacity in excess of 330 mAh/g. This material is used in combination with a positive electrode composed of layered oxides with both O3- and P2-type structures, achieving a reversible specific capacity of 134.5 mAh/g and an ICE of over 90% [57].

Schütte et al. published a work presenting the first Na-ion battery full cell parametrization for use in a physico-chemical model (PCM). PCMs are widely used in battery research, as they can help identify the battery parameters, determine anode potential during fast charging, predict available battery power, model material degradation during cycling, and more. The parametrization was performed on a commercial 1.2 Ah 18,650 cell using hard carbon and layered oxide as electrodes. Their work utilizes already established analysis techniques for LIBs and acknowledges their transferability to SIB cell analyses. It emphasizes the importance of SoC-dependent parameters (such as the diffusion coefficient of hard carbon), thermal models, aging, and hysteresis models, providing guidance for future parameterizations and PCMs in the SIB field [58].

Soft carbon

Soft carbon is a type of carbon with arranged layers and a disordered structure characterized by tight spacing between layers. These short distances prevent Na^+ intercalation, as seen in the work of Cheng et al., where the precursor from pyrene and terephthaloyl chloride is prepared at a ratio of 1:0.5 and subsequently fired at 1300 °C, resulting in the formation of soft carbon with an ordered structure. The C-1:0.5 sample reached a capacity of only 181 mAh/g at a potential of 0.1 V vs. Na/Na^+ . The BET area was 8.2 m^2/g , the percentage of closed pores equaled 0, and the d022 plane distance (narrowest interlayer) was 0.345 nm. A similar sample was formed at a C-1:10 ratio, which resulted in the formation of hard carbon featuring a capacity of 399 mAh/g at a potential of 0.1 V vs. Na/Na^+ , a BET area of 6.4 m^2/g , 70% of closed pores, and a d022 layer distance of 0.382 nm [59]. The difference between the soft- and hard-carbon structures can be seen in Figure 7.

Pendashteh et al. conducted an experiment with soft carbon formed by pyrolysis at 500 °C of PVC (polyvinyl chloride), subsequent treatment with ball milling, and repeated pyrolysis at 800 °C. For this material, a reversible capacity of 207 mAh/g was achieved at a current density of 25 mA/g, a BET measurement area of 5.8 m^2/g , and an ICE of 82%. At a current density of 372 mA/g, this material maintains a capacity of 145 mAh/g, and this capacity does not drop below 100 mAh/g for the duration of 400 cycles [60].

Soft carbon, despite its less demanding production and good stability, offers low capacities. This is caused by the aforementioned interlayer distances. Referring to the Web of Science, lower interest in this material in connection to SIB can be observed (only 75 articles have been published in the last 6 years when searching for “Soft Carbon Na-ion”) [61]. Thus, the use of soft carbon in SIB batteries and stationary storage systems is a

question of future development, as today, there are more promising materials in terms of capacities and current load.

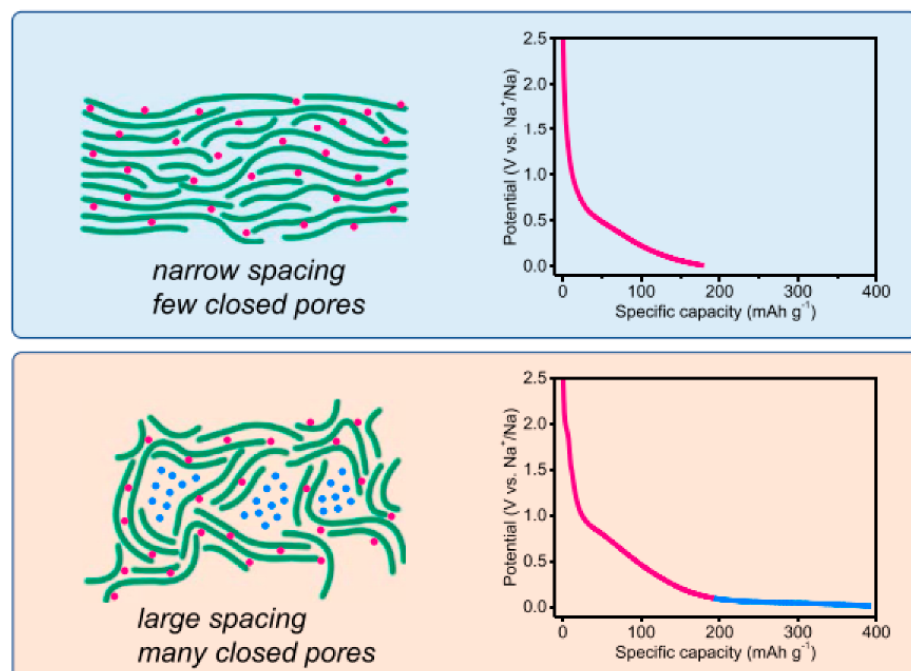


Figure 7. Na⁺ storage mechanism in soft carbon and hard carbon, respectively [59].

Graphene/rGO

Graphene is the most stable allotrope of carbon, consisting of carbon atoms arranged in a hexagonal lattice which together form a layer with a one-atom thickness. The individual layers are attracted to each other by van der Waals forces. The interlayer distance of such layered graphene amounts to 3.35 nm [62].

Graphene exhibits very favorable properties in terms of mechanical strength, electrical conductivity, and high theoretical surface area. However, when only one layer of graphite is used in conjunction with Na⁺, there is a lack of proper absorption of this ion, as it is energetically disadvantageous for graphite, resulting in a decrease in the theoretical capacity [62].

In order to use graphene as a negative-electrode material, it needs to be modified using defects. These defects are meant to disrupt the graphene lattice and create gaps in which Na⁺ can then intercalate. Graphene lattice defects can be divided into two groups. The first group is made up of intrinsic defects, among which are defects caused by vacancies, Thresher–Stone–Wales defects (change in the rotation of the π-bonds of the C=C carbon atoms), and other defects not caused by the presence of foreign atoms. The second group covers extrinsic defects, which are formed by foreign atoms [63,64].

However, these defects also pose the disadvantage of low ICE in the first few cycles. Ding et al. pointed out the importance of the preparation of graphene layers, where low firing temperatures of about 600 °C lead to the formation of graphene with rGO properties, while higher temperatures (1400 °C) lead to graphene with lower porosity and larger interlayer spacing. Despite the higher-quality graphene, the ICE still remains low at around 60% [65].

These defects were used by Wang et al. in the fabrication of a 3D-printed Au/rGO (rGO—reduced graphene oxide) anode by mixing GO with HAuCl₄ compound. The mixture was then washed in deionized water and centrifuged to form an Au/GO ink suitable for 3D printing. After printing, excess water was removed using the freeze-dry

method, leading to the formation of the Au/rGO structure. Prior to use, Na deposition was performed on the material to obtain Na@Au/rGO. Combined with a 3D-printed NVP@C-rGO cathode, this material exhibited a reversible capacity of 91.2 mAh/g at a current load of 100 mA/g. Furthermore, the cell exhibited a reversible capacity of 84.95 mAh/g at a current density of 100 mA/g with high CE (up to 96%) after 205 cycles [66]. This work provides insight into a new method of 3D-printed materials, which is among the areas of interest in the production of electrode materials. Unfortunately, the demanding production of rGO as well as the price of HAuCl₄ may affect their large-scale use, for example, in stationary storage applications.

Sodium titanates

Sodium titanates are of interest due to their stability, material availability, and environmental friendliness. The most well-known sodium titanate is Na₂Ti₃O₇ based on the familiar and commercially used LIB negative-electrode material Li₄Ti₅O₁₂. The basic structure of Na₂Ti₃O₇ consists of a TiO₆ octahedral exhibiting a zigzag layer structure, as shown in Figure 8. The benefit of this material is the low Na⁺ insertion potential (0.3 V vs. Na⁺/Na), providing a higher SIB operating voltage. The drawback of this material is the slow diffusion of Na⁺ ions attributed to the large bandgap voltage of 3.7–3.9 eV [67].

All of this results in low electrochemical activity at higher charging and discharging currents, which limits the use of Na₂Ti₃O₇ in high-power applications. This shortcoming has led to efforts to enhance ion diffusion using a range of doping techniques, nanostructures, fabrication using carbon-based composites, or surface modifications [67,68].

The group of Wang et al. also used nanostructure techniques. To create a negative electrode, they used carbon nanotubes with a diameter of 270 nm, which were then used to prepare Na₂Ti₃O₇ nanowires and nanobelts by synthesizing TiO₂ (titanium dioxide) in NaOH (sodium hydroxide). An example of the final structure can be seen in Figure 8. The material formed by the nanobelts exhibited a surface area of 38.68 m²/g with a capacity of 239 mAh/g at a current density of 0.1 A/g. Moreover, this material achieved high cyclability, with over 5000 cycles at a current density of 10 A/g at 100% capacity retention. Nevertheless, the excellent properties of the negative electrode were diminished by the relatively complex and energy-intensive production of carbon nanofibers (CNF), as their synthesis is performed by electrospinning the material at 15 kV followed by firing at 1000 °C [67].

Zhong et al. used carbon MXene composite Ti₃C₂T_x in the preparation of a negative electrode. Its fabrication utilized a hydrothermal reaction in H₂O₂ (hydrogen peroxide) and NaOH solution to form Na₂Ti₃O₇ materials, followed by calcination in Tris-buffer solution in order to create the Na₂Ti₃O₇@C material. The resulting structure can be observed in Figure 8. Using the BEL method, an area of 132.93 m²/g was calculated. In addition, the material shows a voltage window ranging from 0.01 at charge to 3 V at discharge (vs Na/Na⁺) at a scan rate of 0.1 mV/s on the CV curve. Na₂Ti₃O₇@C exhibits high cyclability at a current density of 2 A/g, reaching a reversible capacity of 119 mAh/g while maintaining 93.5% of its capacity after 200 cycles. While this material fails to achieve the same capacitance and stability as the material of Wang et al., Na₂Ti₃O₇@C has less energy and process-intensive production [69].

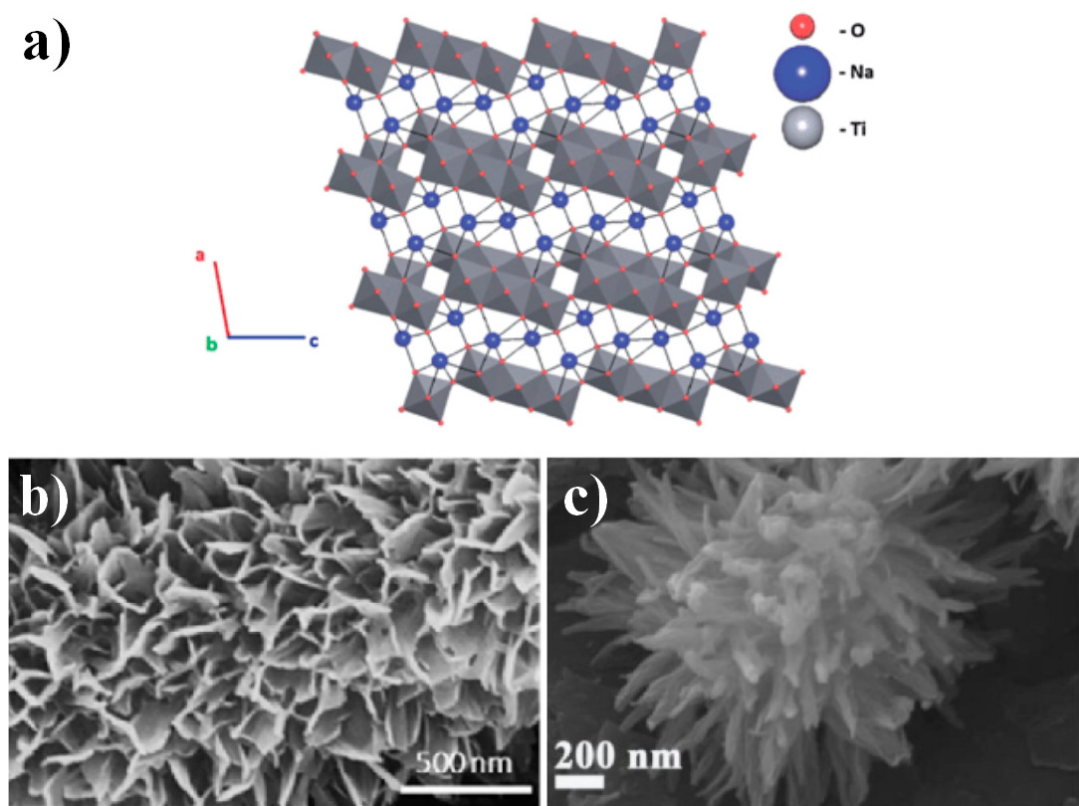


Figure 8. (a) $\text{Na}_2\text{Ti}_3\text{O}_7$ zigzag structure [70]. (b) SEM image of nanobelts/CNF [67]. (c) FESEM (fast emission scanning electron microscopy) image of $\text{Na}_2\text{Ti}_3\text{O}_7$ @C [69].

3.1.2. Alloying and Conversion Materials

Sn-based materials

The use of Sn involves both alloy and conversion reactions for Na^+ deposition. Large volumetric changes occur in alloy materials during sodation and after desodation. This leads to a very rapid capacity loss due to cracking of the SEI layer and its eventual restoration, which reduces the active-electrode material. At the same time, the electrode material undergoes decomposition, manifested by the loss of contact between the electrode and the collector. This results in disconnection of the material from the potential, and its participation in current and capacitance reactions is hindered. Other issues with Sn-based materials are, for example, low ICE and low intrinsic conductivity. These disadvantages result in the inability to develop SIBs with a long lifetime and good safety, mainly due to the unstable SEI layer [71].

In order to limit undesirable volumetric changes, a number of material modifications have been employed, such as nanosizing (modification of and reduction in Sn material particles), combination with carbon materials (carbon nanotubes, graphene, etc.), defects (oxygen or sulfur vacancies), or structural modifications [46,71].

Li et al. used the nanosizing method in combination with carbon material to synthesize Sn-Ni@NC (NC = nitrogen-doped carbon) material. This material exhibited a very high initial capacity of 537.5 mAh/g when discharged and 319.7 mAh/g when charged with an ICE of only 59.47%, which was presumably due to the formation of the SEI layer. At a current load of 0.2 A/g, Sn-Ni@NC maintained a reversible capacity of 264.9 mAh/g compared to the Sn-Ni material, which only reached 141.8 mAh/g. Furthermore, the Sn-Ni@NC material exhibited a reversible capacity of 177.4 mAh/g at a current density of 1 A/g, maintaining a capacity of 148.1 mAh/g after 200 cycles [72].

Sb-based materials

Sb-based materials suffer from the same undesirable properties as Sn-based materials. They employ similar modifications to achieve higher capacities, lower volumetric expansion, and higher electrical conductivity. Yu et al. used intermetallic compounds with antimony ($TiSb_2$ and $NbSb_2$) to synthesize Sb@TiC@C and Sb@NbC@C materials.

The individual materials use amorphous carbon to compensate for volumetric changes. The different materials achieved very high volumetric capacities, with Sb@TiC@C reaching 746 mAh/cm^3 (at a mass of 1.86 g/cm^3 , the gravimetric capacity reaches 401 mAh/g). Furthermore, a volumetric capacity of 726 mAh/cm^3 was achieved for Sb@NbC@C (at a mass of 1.93 g/cm^3 , the gravimetric capacity amounts to 376 mAh/g). This capacity was retained by the materials even after 100 cycles at a current density of 50 mA/g [73].

Pb-based materials

Lead can be classified as a possible negative-electrode material for SIBs. Lead itself has a reversible capacity of up to 464 mAh/g , with 98.5% capacity retention after 50 cycles, at a current density of 13 mA/g . These properties were utilized in an experiment by Pandit et al. in the construction of a full cell made of $Na_3V_2(PO_4)_3/C$ material as a positive electrode and Pb as a negative electrode. The full cell achieved a reversible capacity of 233 mAh/g at a current density of 0.1 C with an excellent energy density of 170 Wh/kg [74]. Recycled Pb, which can be extracted quite successfully from older Pb-acid batteries, could be employed in negative electrodes. The high toxicity and high density of Pb still represent considerable disadvantages [75].

MXene-based materials

MXenes are inorganic materials forming 2D structures from transition metals (commonly carbides, nitrides, and carbonitrides). Some of the characteristic properties of MXene include excellent electrical conductivity, an intrinsic layered structure (aiding in the fast movement of ions), and the possibility of adjusting interlayer distances (allowing for the deposition of different ions or molecules) [76,77].

Tang et al. focused on the confinement of SnP (Tin monophosphide) into the $Ti_3C_2T_x$ MXene structure. By etching the Ti_3AlC_2 material with highly concentrated hydrofluoric acid, $Ti_3C_2T_x$ MXene was prepared (T_x denotes terminal groups H, OH, and F on the surface and edges). Afterwards, positive NH_4^+ ions were introduced into the intergrid spaces of MXene by electrostatic intercalation, resulting in stretching of the interlayer distances from 0.96 nm to 1.21 nm . Next, SnO_2 nanocrystals were formed in the interlayer spaces of MXene using a hydrothermal method. Next, the MXene mixture was manually crushed together with NaH_2PO_2 and fired in an argon atmosphere, resulting in the formation of the SnP phase, and enabling the assembly of the M-SnP-in material. This material achieved a very strong reversible capacity (584.5 mAh/g) at a current density of 0.2 A/g over 200 cycles and 438.2 mAh/g at a current density of 15 A/g . Furthermore, the material exhibited excellent cyclability—maintaining a capacity of 436.6 mAh/g at a current density of 2 A/g for 1500 cycles (the SnP_x alloy material lasted for only 600 cycles, with less than half of its original capacity remaining after 300 cycles). Finally, a full cell was constructed in combination with the cathode material $Na_3V_2(PO_4)_3$, yielding an energy density of 265.4 Wh/kg [76].

3.2. Positive-Electrode Materials

In the last decade, numerous materials have been studied as potential positive-electrode materials for SIBs. The options for positive-electrode materials include layered transition metal oxides, polyanionic compounds (phosphates, fluorophosphates...), Prussian blue derivatives, conversion materials (transition metal fluorides, oxyfluorides,

sulfides, and selenides), and organic compounds [29]. Among these options, the first three listed have been shown to be the most promising [78].

Layered Transition Metal Oxides

Due to their high structural compatibility for Na^+ insertion and extraction, simple structure, ease of synthesis, and high operating potential, layered transition metal oxides (TMOs) are considered to be among the most promising candidates among all considered materials for positive SIB electrodes. Depending on how the sodium ion and transition metal layers are stacked, layered transition metal oxides can have a different structures. P2-type (having higher rate performance and capacity retention) and O3-type phases (able to achieve high capacities) have been shown to be the most interesting in the SIB field. The biggest drawbacks of layered transition oxides are large volume changes caused by phase transitions. Many synthesis methods are used to form layered metal oxides, such as sol–gel, hydrothermal, solid-state, and coprecipitation [29,47]. For example, the sol–gel method is very promising, as it offers the desired structural, morphological, and electrochemical properties, as the homogeneity and purity are easily controlled by selecting suitable precursors. It consists of dissolved Na in transition metal salts in a solvent with an added gel-forming chelating agent. Hydrothermal synthesis uses quite low temperatures, resulting in low energy consumption and ease of synthesis, while solid-state synthesis has the advantage of ease in achieving the right stoichiometry [79]. Along with the quite simple coprecipitation method, the synthesis methods in general are not too complicated and readily attainable [78].

The layered structures are made of edge-sharing TMO_6 ($\text{M} = \text{Fe}, \text{Mn}, \text{Ni}, \text{Co}, \text{Cr}, \text{Ti}, \text{V}$, and their combinations) octahedra, forming repeating layers between which Na^+ ions are positioned in the octahedral (O) oxygen environment, which is called O-type stacking. On top of that, in the case of Na-ion oxides, P-type stacking can occur, where the P-type refers to prismatic Na-ion coordination. The most studied layered stacking configurations are the P2 phase (ABBA oxygen stacking) and the O3 phase (ABCABC oxygen stacking), as seen in Figure 9. P2-type usually provides higher rate performance and good cycling stability when compared to O3-type analogs due to its greater Na ion conductivity and better structural integrity; however, its first charge storage capacity is limited due to the lower initial Na content. It is typical that upon Na ion intercalation and deintercalation during cycling, the structure shifts between O- and P-types, commonly degrading its cycle stability. Metal oxides consisting of more elements (especially those including Mn) tend to provide higher energy densities than those with a single element [80].

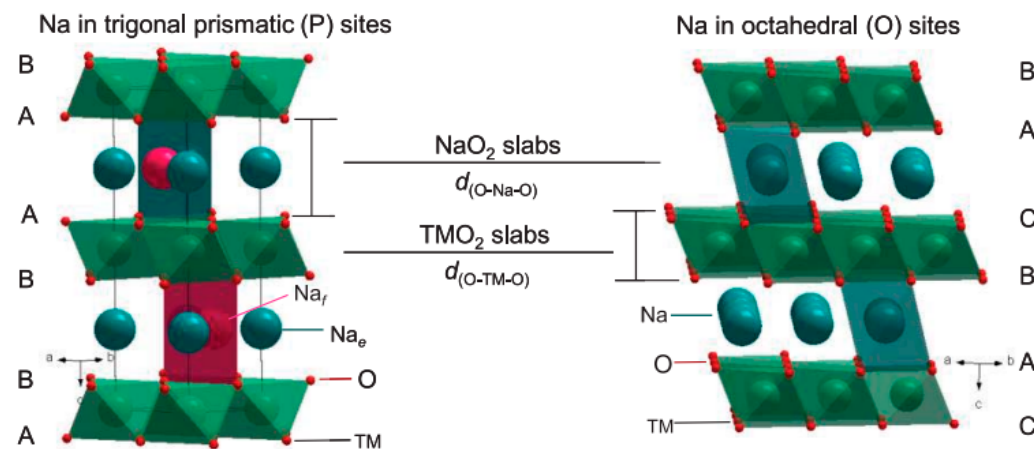


Figure 9. Illustration of crystal representative P2-type and O3-type layered oxides [80].

P2 type $\text{Na}_{2/3}\text{Ni}_{1/3}\text{Mn}_{2/3}\text{O}_2$, for instance, stands out for its high capacity of 160 mAh g^{-1} ; however, its capacity quickly fades after reaching 4.2 V due to the P2-to-O3 phase transition. A layer of the NaPO_3 surface is able to help improve stabilization for long-term cyclability, as it is able to suppress oxygen release in the highly desodiated state of the battery. O3-type $\text{NaNi}_{0.5}\text{Mn}_{0.5}\text{O}_2$ is able to provide capacities in the range of 105–125 mAh/g at 2.2–3.8 V. Zhao et al. prepared a high-entropy O3-type $\text{NaNi}_{0.12}\text{Cu}_{0.12}\text{Mg}_{0.12}\text{Fe}_{0.15}\text{Co}_{0.15}\text{Mn}_{0.1}\text{Ti}_{0.1}\text{Sn}_{0.1}\text{Sb}_{0.04}\text{O}_2$ using a solid-state synthesis method, achieving a reversible capacity of about 110 mAh/g. This material retained 83% of its capacity after 500 cycles and ~80% capacity retention at a 5C rate, operating in the voltage range of 2.0–3.9 V, versus Na^+/Na [78]. O3-type materials could contribute to higher energy densities, while P-2 exhibits higher capacity retention and stability. Both types are promising candidates for low-cost SIB energy storage systems application in the near future, although further research is needed to enhance the performance of these materials [47].

Extensive research has been performed on both O3- and P2-type layered structures. In 2013, $\text{Na}_{0.950}\text{Ni}_{0.317}\text{Mn}_{0.317}\text{Mg}_{0.158}\text{Ti}_{0.208}\text{O}_2$ material with a typical O3 phase provided high energy and a good cycle life; however, no further developments were made at the material level. Eventually, a mixed-phase material was developed, averaging the stoichiometries of O3- and P2-type materials. The stoichiometries used were $\text{Na}_{0.667}\text{Ni}_{0.300}\text{Mn}_{0.600}\text{Mg}_{0.033}\text{Ti}_{0.067}\text{O}_2$ for the P-type and $\text{NaNi}_{0.333}\text{Mn}_{0.033}\text{Mg}_{0.167}\text{Ti}_{0.167}\text{O}_2$ for the O3-type (an image of the stacked morphologies can be seen in Figure 10). The material delivers a capacity of 156 mAh/g at 0.2C in the 4.35–2 V window. It also retains 80% of its capacity after 3000 cycles and allows for charging at 4C without capacity drops when paired with hard carbon in a pouch cell [57].

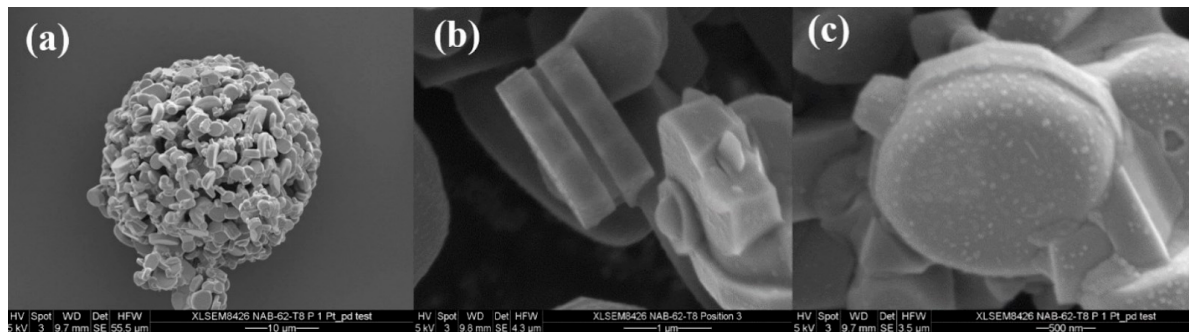


Figure 10. FESEM images of the combined stoichiometries of the Faradion positive-electrode material. (a) A zoomed-out image. (b,c) Magnified images showing the stacked O3/P2 phase morphologies of the primary particles [57].

Polyanion-type materials

Owing to the stability of their crystal structure, thermal stability, adjustable voltage, and high ionic conductivity, polyanion-type materials seem to be a strong candidate for positive-electrode materials used in SIBs. The main obstacles with these materials are low electron conductivity, unsatisfactory theoretical specific capacity, and low energy density. The structure of these materials is composed of MO_x polyhedral ($\text{M} = \text{metal}$) and anion groups (XO_4^{n-} ($\text{X} = \text{B}, \text{C}, \text{S}, \text{P}, \text{Si}, \text{As}$, etc.) or their derivatives connected by a covalent bond [81]. The most commonly adopted material synthesis methods are the sol-gel and the solid-solid method. The sol-gel method allows for the synthesis of materials with a high surface area and allows for properties such as homogeneity and purity to be easily controlled, but controlling the pore structure and morphology is quite problematic. The solid-state technique provides many benefits, such as low cost and simple equipment

requirements; however, it provides minimal control over the morphology and shape of the material, influencing the final electrochemical performance [82].

Among polyanionic compounds, NASICONs (Na Super Ionic Conductors) are a subject of interest thanks to their strong 3D framework, high rate capability, long cyclability, and satisfactory kinetics of sodium-ion mobility, making them suitable for high-power applications. NASICONs used as positive electrodes are generally phosphates combined with various transition metals, such as vanadium (V), iron (Fe), and manganese (Mn). Combinations of these metals may be used as well [29]. $\text{Na}_3\text{V}_2(\text{PO}_4)_3$ (NVP) is a typical example of a NASICON structure, with a specific capacity of 117 mAh/g and a voltage plateau at ~3.5 V. Zhao et al. analyzed the $\text{Na}_4\text{MnCr}(\text{PO}_4)_3$ structure, which retained 85% of its capacity after 500 cycles at 100 mA/g at a cutoff potential of 4.3 V, meaning the energy density at the highest potential is over 400 Wh/kg [83]. Hu et al., for instance, constructed NASICON-type $\text{Na}_{3.2}\text{MnTi}_{0.8}\text{V}_{0.2}(\text{PO}_4)_3$, with five redox couples ranging from 2.1 to 4.1 V, showing a capacity of 172.5 mAh/g and quite a high energy density of 527.2 Wh/g [84].

Fluorophosphates, such as $\text{Na}_3\text{V}_2(\text{PO}_4)_2\text{F}_3$ (NVPF), are the subject of extended studies. They offer a theoretical capacity of roughly 128 mAh/g and a working voltage of ~3.9 V, achieving an energy density of ~506 Wh/kg. However, they suffer from capacity fading at high rates due to low conductivity and insufficient ion diffusivity [39,85]. Gu et al. prepared a $\text{Na}_3\text{V}_{1.98}\text{Mn}_{0.02}(\text{PO}_4)_2\text{F}_3$ electrode material using a hydrothermal synthesis method, which offers a specific capacity of 123.8 mAh/g at 0.1C in the voltage range from 2.0 to 4.3 V versus higher than Na^+/Na , and power density around 400 Wh/kg [85,86].

Plewa et al. synthesized $\text{Na}_2\text{FeM}(\text{SO}_4)_3$ ($\text{M} = \text{Fe}, \text{Mn}, \text{Ni}$) nanometric size grain materials through the uncomplicated dissolution of Na_2SO_4 and transition metal sulfates in a liquid solution, subsequent solvent evaporation, and annealing. All of the tested $\text{Na}_2\text{FeM}(\text{SO}_4)_3/\text{C}$ cells represented systems of high voltage >3.6 V with a capacity of 110 mAh/g (and therefore an energy density of over 396 Wh/kg) and capacity retention of 90% after 50 cycles [87]. While polyanion-type materials offer advantages in terms of voltage, thermal stability, and cycle life, their lower specific capacity might not be suitable for energy-dense applications. NVPs are, for instance, suitable for high-power batteries (rather than energy-dense ones) as they exhibit fast electrochemical kinetics at the cost of quite low specific capacities [45].

Prussian Blue Materials

Prussian blue analogs (PBAs) represent high-entropy electrode materials from the family of metal–organic frameworks (MOFs). Prussian blue suffers from low Coulombic efficiency and capacity fading, but offers a high theoretical capacity, and its framework provides enough space for Na^+ insertion and extraction. Thanks to its high rate capability and satisfactory cycling stability, it can be suitable for high-power applications [29,88]. PBAs exhibit face-centered cubic structures and are described by the molecular formula $\text{Na}_x\text{M}[\text{Fe}(\text{CN})_6]_{1-y} \cdot {}^*\text{y} \cdot \text{mH}_2\text{O}$, where M stands for transition metal elements (Fe, Co, Ni, and Mn). Here, * denotes $[\text{Fe}(\text{CN})_6]$ defects, where the range of x is $0 < x < 2$, and the range of y is $0 < y < 1$. M-based PBs (apart from Ni) show a theoretical capacity of up to 170 mAh/g; however, the $[\text{Fe}(\text{CN})_6]$ defects generated during the synthesis process alongside crystalline water cause lattice distortion and structural collapse during the cycling process, resulting in a reduction in capacity and cycling performance [89]. In terms of theoretical capacity, this material can be compared to commercially used positive-electrode LIB materials, where LiCoO_2 has a theoretical capacity of 274 mAh/g (practical discharge capacity of 173 mAh/g with acceptable reversibility), LiFePO_4 shows a theoretical capacity of 154 mAh/g, and LiMn_2O_4 achieves 148 mAh/g [90–92]. In general, PBAs are a promising class of materials for energy storage applications, with Fe-based PBAs standing out as

the most environmentally friendly option owing to their use of abundant, non-toxic, and sustainable elements [89].

Hydrothermal, coprecipitation, and electrodeposition methods are the most popular synthesis techniques employed in electrochemical applications. In the widely used hydrothermal method, the morphology of PBA is determined by the used precursor structure. The coprecipitation approach is used by many because of its simplicity and low cost; however, it does not allow for adjustment of the crystal shape and size as well as the hydrothermal method. As for the electrodeposition method, the utilized substrate greatly influences the morphology of the final electrode material [93].

To address the issues of $\text{Fe}(\text{CN})_6$ defects, Wang et al. developed a hollow layered Fe-PB composite using the hydrothermal synthesis method. 1,3,5-benzene tricarboxylic acid (BTA) was utilized as a chelating and etching agent as its carboxyl groups (-COOH) can chelate with Fe_2^{+} ions, so high-quality cubic Fe-PB can be produced by controlling the reaction rate of Fe-PB formation. The hollow layered structure was shown to significantly reduce the diffusion path of Na^{+} ions and limit the volume changes during Na-ion insertion/extraction. The electrode's initial discharge capacity equaled 95.9 mAh/g and remained at 73.1 mAh/g after 500 cycles in the voltage range of 2.0–4.2 V. The full cell paired with hard carbon provided a considerable energy density of 312.2 Wh/kg [89].

There are many PBA modification methods, among which metal-ion doping (doped at the M-site or Na-site) is currently one of the most effective modification methods, with the goal of reducing $\text{Fe}(\text{CN})_6$ vacancies. Chen et al. directly prepared a Cu-doped Fe-PBA using the coprecipitation synthesis method. The resulting material contained fewer $\text{Fe}(\text{CN})_6$ vacancies and low crystal water content. The added Cu contributed to structure stability, allowing the material to achieve an initial capacity of 127.4 mAh/g (while undoped Fe-PBA achieved 107.9 mAh/g) at 100 mA/g between 2.5 and 4.2 V. Cu doping is therefore an effective modification method, improving the overall performance of PBA positive-electrode materials [94].

PBA-based SIBs can be put between supercapacitors and other batteries (Ni-Cd, lead-acid, LIBs) in terms of cycle life and power density (up to 1250 W/kg). As they have the highest cycle number (>40,000 cycles) among all batteries and use abundant, non-toxic raw materials, they could be an alternative for energy storage in high-power applications, including backup power for data centers and regenerative braking. An example of the commercial use of these batteries is the PBA-based pluggable sodium-ion module (four-cell stacks in series connection) developed by ABB and Natron. The utilized iron-based PB electrode material can be seen in Figure 11. These cells were subjected by He et al. to UL 9540A thermal runaway tests, comprising external short-circuit tests, external heating, and mechanically induced events (e.g., nail penetration). None of these tests triggered thermal runaway, demonstrating the SIBs' safety. Their energy density sits quite low (23 Wh/kg at the cell level), but they show high rate capability and very satisfactory capacity retention [95]. Another example is SIB prototype cells by Novasis Energies, Inc., using a PBA positive electrode, commercial hard-carbon negative electrode, and a nonaqueous (e.g., salts dissolved in non-water-based solvents) electrolyte. This company was able to construct 0.5–5 Ah capacity high-safety pouch cells with noteworthy rate capabilities and cycle life [96].

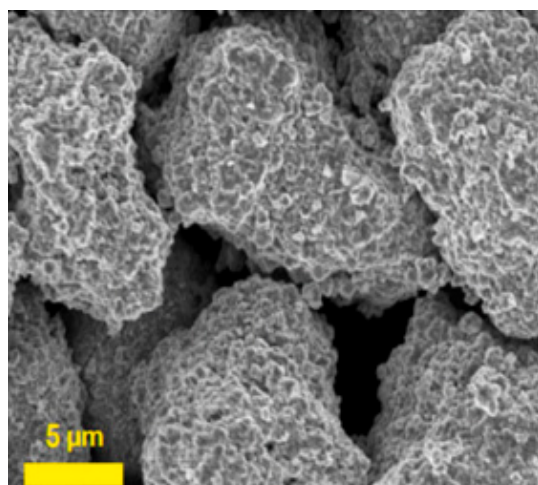


Figure 11. SEM image of Natron iron-based positive-electrode material $\text{Na}_x\text{Mn}_y\text{Fe}(\text{CN})_6\cdot\text{nH}_2\text{O}$ [95].

Organic materials

Organic-based positive-electrode materials have attracted considerable attention, as they are made up of weak intermolecular interactions (e.g., hydrogen bonds and van der Waals forces), which results in a flexible structure capable of accommodating Na^+ ions without significant volume change while allowing their smooth transport. They can be divided into two groups—carbonyl small molecules (ketones and quinones, anhydride compounds, imide compounds, and carboxylate compounds) and organic polymers (carbonyl and conjugated conductive polymers, covalent organic frameworks (COFs), organometallic compounds, and organic radial polymers). Organic compounds have the advantages of low toxicity, structural diversity, ease of synthesis, and material abundance tied to sustainability. They suffer from electrolyte dissolution, low stability, and poor electronic conductivity, preventing their utilization in practice [97].

To tackle these issues, Kuan et al. reported the use of nitrogen- and carbonyl-rich highly extended p-conjugated small organic molecule hexaazatrianthrylene (HATA) embedded quinone (HATAQ). HATAQ molecules create supramolecular graphite-like 2D layered arrangements in the solid state, promoting charge transfer and helping to improve structural stability. The material, when combined with Na metal negative electrodes in a coin cell, demonstrated a 460 mAh/g capacity at 500 mA/g (1C) and retained 99% of its capacity (138 mA) after 5000 cycles at 60 A/g, which is one of the top reported values for organic small molecules so far. The estimated gravimetric energy density is estimated to be 920 Wh/kg, based on the specific capacity obtained at 1C and an average discharge potential of 2.0 V [97].

Metal–organic polymers (MOPs) have been subjected to many studies on conjugated carbonyl-derived linkers, as they offer multiple redox centers and are low-cost. Wang et al. synthesized a flower-like p-d conjugated MOP (copper–tetramino–benzoquinone, Cu-TABQ) where TABQ serves as an organic ligand and Cu_2^+ as a transition metal node. Both elements act as dual redox centers, allowing the achievement of a reversible capacity of 322.9 mAh/g at 50 mA/g in the voltage range of 1.0–3.0 V (meaning the average power density revolves around 645.8 Wh/kg). With an ICE of 75.6%, the electrode material retained 98.7% of its capacity after 50 cycles. Owing to the stable coordination between Cu_2^+ and TABQ, the positive-electrode electronic conductivity and Na^+ redox reaction were significantly improved, so the capacity reached 198.8 mAh/g even at a high current density of 4000 mA/g [98].

Due to their structure, organic materials have the potential to be used in applications where light weight, portability, and flexibility are crucial. If the mentioned limitations can

be effectively mitigated, organic materials could emerge as promising electrode materials, especially in renewable and environmentally responsible organic batteries [3].

3.3. Electrolytes and Salts

Electrolyte research is focused on non-flammable electrolytes with applications in a large temperature range. As for stationary SIB applications, finding electrolytes with properties that would help reduce additional costs regarding the heating, fire safety, etc., of the area where the battery is stored is needed. In addition, such materials must not significantly increase the battery's cost [29].

SIBs can be used with liquid or solid electrolytes. The liquid electrolyte is the medium used to transfer the charge (Na^+ ions) from the negative to the positive electrode and vice versa. The most commonly used liquid electrolytes are electrolytes based on salts dissolved in organic aprotic solvents (mainly based on ethers, esters, and carbonates). As for solid-state electrolytes (SSE), polymeric bonds with sodium salts are the most common type. Furthermore, there are also inorganic solid electrolytes (ISEs) consisting of oxides, phosphates, sulfates, and hydrates. ISEs are hard, inflexible materials that are mainly used in high-temperature Na-S systems [29].

Individual electrolytes may differ in terms of their working temperature range, solubility of sodium salts, and Na^+ transfer rate. Du et al. compared ether-based non-flammable electrolytes (1 M NaBF_4 in tetraglyme) with carbonate-based electrolytes (1 M NaClO_4 in 1:1 ethylene carbonate (EC)/propylene carbonate (PC)) in HC half-cells in a voltage range of 0.001–1.5 V. At 0.2 C, the HC achieved a high initial charge capacity of 273 mAh/g, ICE of 87%, and 99% capacity retention after 50 cycles using 1 M NaBF_4 in tetraglyme. The carbonate-based, 1 M NaClO_4 in EC/PC electrolyte only reached 178 mAh/g, and exhibited lower ICE of 69% and capacity retention of 84%. It is worth noting that the ether-based electrolyte achieved a considerable charge capacity of 223 mAh/g at a 2C rate. For this material, Differential Scanning Calorimetry (DSC) showed higher onset temperatures for the first exothermic peak (SEI cracking), which implies higher thermal stability. The non-flammable nature of the ether-based electrolyte can reduce the need for extensive safety measures in battery system storage. Along with the electrolyte's contribution to the battery's long lifespan, the overall costs may be lowered, which is a critical aspect for battery systems in stationary applications [99].

The development of aqueous SIBs is likely to be limited by their low energy density and unsatisfying output potential due to the low electrochemical stability window of the electrolyte (only 1.23 V under thermodynamic conditions). In addition, aqueous electrolytes suffer from decomposition with hydrogen and oxygen evolution, resulting in poor cycling stability [100].

SSEs are a non-flammable type of electrolyte, which eliminates the risk of fire hazards and enhances the overall safety of the battery system. This is due to the high reactivity of sodium, which could lead to a severe reaction with organic liquid electrolytes. SSEs exhibit high thermal stability, wide electrochemical stability windows, and exceptional mechanical properties [1,38]. This means they can withstand higher voltages without decomposing, leading to increased energy density without compromising safety. Due to their solid nature, SSEs can act as a more effective barrier against dendrites than porous separators in liquid electrolytes, as they can be pierced causing a short-circuit in the cell [40]. Although SSEs are more costly in terms of manufacturing and integration than liquid electrolytes, their extended lifetime and low maintenance could reduce costs in the long run. This, among other characteristics, could be advantageous, especially in stationary applications where the size and weight of the battery are not as critical compared to other fields of application [1]. SSEs can be divided into multiple types, such as solid polymer electrolytes

(SPEs), composite solid polymer electrolytes (CSPEs), and inorganic solid electrolytes (ISEs). All of these types have their unique characteristics and are under active development. In the present day, ISEs (among which $\beta''\text{-Al}_2\text{O}_3$ (beta alumina) and NASICON $\text{Na}_3\text{Zr}_2\text{Si}_2\text{PO}_{12}$ are the most used) are recognized for their high ionic conductivity and are frequently employed in high-temperature Na/S batteries [29].

3.4. Separators

A wide operating temperature range and non-flammability are among the key qualities of separators. In addition, the porosity and wettability of separators are equally as important, as they affect the internal resistivity of the battery and affect its general performance [101].

The most widely used separator materials in SIB applications include polyolefin-based materials. This group contains, for example, polypropylene (PP), polyethylene (PE), and glass fiber (GF). These materials are mainly used for their chemical stability and inexpensive large-scale production. The disadvantages of PP and PE include poor wettability and insufficient electrolyte retention when used with carbon-based electrolytes, e.g., propylene carbonate (PC), ethylene carbonate (EC), and dimethyl carbonate (DMC). Another drawback is the low temperature range of PP and PE (their melting points are at 165 °C and 132 °C, respectively). The greatest potential danger to the battery is the material's expansion—at higher temperatures, PP and PE tend to shrink, leading to internal short-circuits and other critical issues. As far as GF separators are concerned, the thickness of the material and its arrangement are not ideal. Due to the high porosity of GF, a larger amount of electrolyte is needed for filling and poses a risk in the case of dendrite formation [102–105]. Separators based on cellulose can also be found, as it is the most widely used biopolymer (plant biomass consists of 40–45 wt% of cellulosic content). It represents a very promising material in the field of renewable materials, with numerous applications, including energy storage systems. The downsides of cellulose-based separators include their flammability and moisture content (depending on the manufacturing process); however, they are highly available and affordable [106].

Aquion Energy, Inc., a company developing aqueous SIBs as an alternative to LIBs and other systems for grid storage, uses a fire-safe seawater solution as an electrolyte and a synthetic cotton separator for their batteries. The output potential of each cell would be limited, however, as cells utilizing aqueous electrolytes suffer from a low electrochemical stability window [107]. Faradion Limited uses low-viscosity nonaqueous liquid electrolytes along with commercially widely used polyolenic separators to stay consistent with established Li-ion cell manufacturing practices [99].

Unfortunately, the development of separators for SIBs has not received nearly as much attention as the development of separators for LIBs. Although LIBs and SIBs work on the same principle, different materials are used, as Na^+ exhibits different kinetic properties compared to Li^+ . It may be beneficial to investigate the suitability of LIB separators in SIBs in the future, as they operate in similar temperature conditions and may utilize electrolytes based on similar principles (e.g., salts in solvent— LiPF_6 for Li-ion, NaPF_6 for Na-ion), etc.

4. Conclusions

SIBs have come a long way since the beginning of their development, and are still being advanced by introducing new materials, improving existing materials, and reducing their environmental impact. Their impact is related both to the use of materials associated with unethical mining practices (e.g., Co) and to materials used in electrodes, such as PVDF binders (requiring the use of the toxic volatile solvent methylpyrrolidone (NMP)) [108]. Fluorine contained in, e.g., PVDF and electrolyte salts poses a significant risk, especially at

elevated temperatures, where toxic gases, particularly highly toxic hydrogen fluoride, can be released when the battery catches on fire. For this reason, alternatives to this element are being actively explored, not limited to the battery industry [109]. The production of SIBs is cost-effective due to the use of Na, which is the most abundant alkaline element in the Earth's crust (2.36% of the continental crust), and also because of the possibility of substituting Cu used in LIBs (\$9.1/kg) with Al (USD 2.5/kg) for current collectors [11,12].

However, there is a limited range of usable materials due to the difficulty of production and the possibility of scaling up. For example, the 3D-printed Au/rGO negative-electrode material is very appealing from an electrochemical point of view, but it is not suitable for mass production. Among the negative-electrode materials with the greatest scale-up potential, HC can be considered due to its simple pyrolytic production from biological materials (shells, algae, wood). PB belongs to the category of very promising positive-electrode materials, with the possibility of hydrothermal synthesis using available materials, such as Fe, Mn, and Ni. In the commercial sphere, the current development of Na-Ion batteries is moving towards the use of widely studied HC and PB electrode materials owing to their high capacities, cycling stability, and environmental friendliness. Regarding electrolytes, great efforts have been made towards the development of SSEs that allow for the application of sodium metal electrode materials. To date, however, the most used types of electrolytes are aprotic solvents (EC/PC or EC/DMC) combined with sodium salts.

The availability and ease of production of electrode and electrolyte materials, along with the ability to avoid less ideal materials like Co and Au, could pave the way for cheaper production and the commercial implementation of sodium-ion batteries (SIBs) in stationary storage facilities, ranging from small- to large-scale. These batteries would help ensure the stability of power grids while reducing environmental impact. However, this is still a theoretical near-future development of SIBs (initial prototypes and applications already exist), as challenges such as the operating temperature ranges, safety, cyclability, and current loads of battery systems have to be addressed.

Author Contributions: Conceptualization, P.B. and J.L.; Methodology, P.B. and J.L.; Validation, P.B. and J.L.; Formal Analysis, S.G. and J.P.; Investigation, S.G. and J.P.; Resources, S.G. and J.P.; Data Curation, S.G. and J.P.; Writing—Original Draft Preparation, S.G. and J.P.; Writing—Review and Editing, P.B., J.L., S.G. and J.P.; Visualization, S.G. and J.P.; Supervision, P.B. and J.L.; Project Administration, P.B. and J.L. All authors have read and agreed to the published version of the manuscript.

Funding: This research was supported by the specific graduate research of the Brno University of Technology No. FEKT-S-23-8286.

Data Availability Statement: No new data were created or analyzed in this study. Data sharing is not applicable to this article.

Conflicts of Interest: The authors declare no conflicts of interest.

References

1. Hirsh, H.S.; Li, Y.; Tan, D.H.S.; Zhang, M.; Zhao, E.; Meng, Y.S. Sodium-Ion Batteries Paving the Way for Grid Energy Storage. *Adv. Energy Mater.* **2020**, *10*, 2001274. [[CrossRef](#)]
2. Dell, R.M. Batteries: Fifty years of materials development. *Solid State Ion.* **2000**, *134*, 139–158. [[CrossRef](#)]
3. Yang, X.; Rogach, A.L. Anodes and Sodium-Free Cathodes in Sodium Ion Batteries. *Adv. Energy Mater.* **2020**, *10*, 2000888. [[CrossRef](#)]
4. Armand, M.; Tarascon, J.-M. Building better batteries. *Nature* **2008**, *451*, 652–657. [[CrossRef](#)] [[PubMed](#)]
5. Olabi, A.G.; Abbas, Q.; Shinde, P.A.; Abdelkareem, M.A. Rechargeable batteries: Technological advancement, challenges, current and emerging applications. *Energy* **2023**, *266*, 126408. [[CrossRef](#)]
6. Huang, Y.; Li, J. Key Challenges for Grid-Scale Lithium-Ion Battery Energy Storage. *Adv. Energy Mater.* **2022**, *12*, 2202197. [[CrossRef](#)]
7. DOE Global Energy Storage Database. Available online: <https://gesdb.sandia.gov/statistics.html> (accessed on 9 January 2025).

8. Usiskin, R.; Lu, Y.; Popovic, J.; Law, M.; Balaya, P.; Hu, Y.-S.; Maier, J. Fundamentals, status and promise of sodium-based batteries. *Nat. Rev. Mater.* **2021**, *6*, 1020–1035. [CrossRef]
9. Battery Grade Sodium Carbonate Price. Available online: <https://www.metal.com/Sodium-ion%20Battery/202404290001> (accessed on 19 November 2024).
10. Lithium Carbonate Price. Available online: <https://www.metal.com/Lithium/201102250059> (accessed on 19 November 2024).
11. Copper Price. Available online: <https://markets.businessinsider.com/commodities/copper-price> (accessed on 19 November 2024).
12. Aluminum Price. Available online: <https://markets.businessinsider.com/commodities/aluminum-price> (accessed on 19 November 2024).
13. Ge, P.; Fouletier, M. Electrochemical intercalation of sodium in graphite. *Solid State Ion.* **1988**, *28–30*, 1172–1175. [CrossRef]
14. Hasa, I.; Dou, X.; Buchholz, D.; Shao-Horn, Y.; Hassoun, J.; Passerini, S.; Scrosati, B. A sodium-ion battery exploiting layered oxide cathode, graphite anode and glyme-based electrolyte. *J. Power Sources* **2016**, *310*, 26–31. [CrossRef]
15. Yabuuchi, N.; Kubota, K.; Dahbi, M.; Komaba, S. Research Development on Sodium-Ion Batteries. *Chem. Rev.* **2014**, *114*, 11636–11682. [CrossRef]
16. Zhang, W.; Zhang, F.; Ming, F.; Alshareef, H.N. Sodium-ion battery anodes: Status and future trends. *EnergyChem* **2019**, *1*, 100012. [CrossRef]
17. Wu, Y.; Shuang, W.; Wang, Y.; Chen, F.; Tang, S.; Wu, X.-L.; Bai, Z.; Yang, L.; Zhang, J. Recent Progress in Sodium-Ion Batteries: Advanced Materials, Reaction Mechanisms and Energy Applications. *Electrochem. Energy Rev.* **2024**, *7*, 17. [CrossRef]
18. Kim, H. Sodium-Ion Battery: Can It Compete with Li-Ion? *ACS Mater. Au* **2023**, *3*, 571–575. [CrossRef] [PubMed]
19. Stevens, D.A.; Dahn, J.R. High Capacity Anode Materials for Rechargeable Sodium-Ion Batteries. *J. Electrochem. Soc.* **2000**, *147*, 1271. [CrossRef]
20. Zhu, Y.; Han, X.; Xu, Y.; Liu, Y.; Zheng, S.; Xu, K.; Hu, L.; Wang, C. Electrospun Sb/C Fibers for a Stable and Fast Sodium-Ion Battery Anode. *ACS Nano* **2013**, *7*, 6378–6386. [CrossRef] [PubMed]
21. Kim, Y.; Park, Y.; Choi, A.; Choi, N.-S.; Kim, J.; Lee, J.; Ryu, J.H.; Oh, S.M.; Lee, K.T. An Amorphous Red Phosphorus/Carbon Composite as a Promising Anode Material for Sodium Ion Batteries. *Adv. Mater.* **2013**, *25*, 3045–3049. [CrossRef] [PubMed]
22. Xiong, H.; Slater, M.D.; Balasubramanian, M.; Johnson, C.S.; Rajh, T. Amorphous TiO₂ Nanotube Anode for Rechargeable Sodium Ion Batteries. *J. Phys. Chem. Lett.* **2011**, *2*, 2560–2565. [CrossRef]
23. Senguttuvan, P.; Rousse, G.; Seznec, V.; Tarascon, J.-M.; Palacín, M.R. Na₂Ti₃O₇: Lowest Voltage Ever Reported Oxide Insertion Electrode for Sodium Ion Batteries. *Chem. Mater.* **2011**, *23*, 4109–4111. [CrossRef]
24. Ellis, L.D.; Hatchard, T.D.; Obrovac, M.N. Reversible Insertion of Sodium in Tin. *J. Electrochem. Soc.* **2012**, *159*, A1801–A1805. [CrossRef]
25. Wang, W.; Liu, X.H.; Mao, S.X.; Huang, J.Y. Microstructural Evolution of Tin Nanoparticles during In Situ Sodium Insertion and Extraction. *Nano Lett.* **2012**, *12*, 5897–5902. [CrossRef] [PubMed]
26. Hariharan, S.; Saravanan, K.; Balaya, P. A-MoO₃: A high performance anode material for sodium-ion batteries. *Electrochem. Commun.* **2013**, *31*, 5–9. [CrossRef]
27. Xie, Y.; Dall’Agnese, Y.; Naguib, M.; Gogotsi, Y.; Barsoum, M.W.; Zhuang, H.L.; Kent, P.R.C. Prediction and Characterization of MXene Nanosheet Anodes for Non-Lithium-Ion Batteries. *ACS Nano* **2014**, *8*, 9606–9615. [CrossRef] [PubMed]
28. Zhang, F.; Alhajji, E.; Lei, Y.; Kurra, N.; Alshareef, H.N. Highly Doped 3D Graphene Na-Ion Battery Anode by Laser Scribing Polyimide Films in Nitrogen Ambient. *Adv. Energy Mater.* **2018**, *8*, 1800353. [CrossRef]
29. Goikolea, E.; Palomares, V.; Wang, S.; de Larramendi, I.R.; Guo, X.; Wang, G.; Rojo, T. Na-Ion Batteries—Approaching Old and New Challenges. *Adv. Energy Mater.* **2020**, *10*, 2002055. [CrossRef]
30. Xu, X.; Zhang, Y.; Sun, H.; Zhou, J.; Yang, F.; Li, H.; Chen, H.; Chen, Y.; Liu, Z.; Qiu, Z.; et al. Progress and Perspective: MXene and MXene-Based Nanomaterials for High-Performance Energy Storage Devices. *Adv. Electron. Mater.* **2021**, *7*, 2000967. [CrossRef]
31. Linden, D.; Reddy, T.B. (Eds.) *Handbook of Batteries*, 3rd ed.; McGraw-Hill: New York, NY, USA, 2002.
32. Zhang, W.; Cao, P.; Li, L.; Yang, K.; Wang, K.; Liu, S.; Yu, Z. Carbon-encapsulated 1D SnO₂/NiO heterojunction hollow nanotubes as high-performance anodes for sodium-ion batteries. *Chem. Eng. J.* **2018**, *348*, 599–607. [CrossRef]
33. May, G.J.; Davidson, A.; Monahov, B. Lead batteries for utility energy storage: A review. *J. Energy Storage* **2018**, *15*, 145–157. [CrossRef]
34. Zhu, Q.; Cheng, M.; Zhang, B.; Jin, K.; Chen, S.; Ren, Z.; Yu, Y. Realizing a Rechargeable High-Performance Cu-Zn Battery by Adjusting the Solubility of Cu²⁺. *Adv. Funct. Mater.* **2019**, *29*, 1905979. [CrossRef]
35. Posada, J.O.G.; Rennie, A.J.R.; Villar, S.P.; Martins, V.L.; Marinaccio, J.; Barnes, A.; Glover, C.F.; Worsley, D.A.; Hall, P.J. Aqueous batteries as grid scale energy storage solutions. *Renew. Sustain. Energy Rev.* **2017**, *68*, 1174–1182. [CrossRef]
36. Zhang, Y.; Mu, Z.; Lai, J.; Chao, Y.; Yang, Y.; Zhou, P.; Li, Y.; Yang, W.; Xia, Z.; Guo, S. MXene/Si@SiOx@C Layer-by-Layer Superstructure with Autoadjustable Function for Superior Stable Lithium Storage. *ACS Nano* **2019**, *13*, 2167–2175.

37. Bommier, C.; Surtia, T.W.; Dolgos, M.; Ji, X. New Mechanistic Insights on Na-Ion Storage in Nongraphitizable Carbon. *Nano Lett.* **2015**, *15*, 5888–5892. [CrossRef] [PubMed]
38. Hasa, I.; Mariyappan, S.; Saurel, D.; Adelhelm, P.; Koposov, A.Y.; Masquelier, C.; Croguennec, L.; Casas-Cabanas, M. Challenges of today for Na-based batteries of the future: From materials to cell metrics. *J. Power Sources* **2021**, *482*, 228872. [CrossRef]
39. Fang, H.; Gao, S.; Zhu, Z.; Ren, M.; Wu, Q.; Li, H.; Li, F. Recent Progress and Perspectives of Sodium Metal Anodes for Rechargeable Batteries. *Chem. Res. Chin. Univ.* **2021**, *37*, 189–199. [CrossRef]
40. Gebert, F.; Knott, J.; Gorkin, R.; Chou, S.-L.; Dou, S.-X. Polymer electrolytes for sodium-ion batteries. *Energy Storage Mater.* **2021**, *36*, 10–30. [CrossRef]
41. Nikiforidis, G.; van de Sanden, M.C.M.; Tsampas, M.N. High and intermediate temperature sodium–sulfur batteries for energy storage: Development, challenges and perspectives. *RSC Adv.* **2019**, *9*, 5649–5673. [CrossRef] [PubMed]
42. Li, M.; Lu, X.; Zhan, X.; Engelhard, M.H.; Bonnett, J.F.; Polikarpov, E.; Jung, K.; Reed, D.M.; Sprenkle, V.L.; Li, G. High performance sodium-sulfur batteries at low temperature enabled by superior molten Na wettability. *Chem. Commun.* **2021**, *57*, 45–48. [CrossRef] [PubMed]
43. Seredych, M.; Shuck, C.E.; Pinto, D.; Alhabeb, M.; Precetti, E.; Deysher, G.; Anasori, B.; Kurra, N.; Gogotsi, Y. High-Temperature Behavior and Surface Chemistry of Carbide MXenes Studied by Thermal Analysis. *Chem. Mater.* **2019**, *31*, 3324–3332. [CrossRef]
44. Desai, P.; Huang, J.; Foix, D.; Tarascon, J.-M.; Mariyappan, S. Zero volt storage of Na-ion batteries: Performance dependence on cell chemistry! *J. Power Sources* **2022**, *551*, 232177. [CrossRef]
45. Pu, X.; Wang, H.; Zhao, D.; Yang, H.; Ai, X.; Cao, S.; Chen, Z.; Cao, Y. Recent Progress in Rechargeable Sodium-Ion Batteries: Toward High-Power Applications. *Small* **2019**, *15*, 1805427. [CrossRef]
46. Wu, C.; Zhu, G.; Wang, Q.; Wu, M.; Zhang, H. Sn-based nanomaterials: From composition and structural design to their electrochemical performances for Li- and Na-ion batteries. *Energy Storage Mater.* **2021**, *43*, 430–462. [CrossRef]
47. Liu, Q.; Hu, Z.; Chen, M.; Zou, C.; Jin, H.; Wang, S.; Chou, S.-L.; Dou, S.-X. Recent Progress of Layered Transition Metal Oxide Cathodes for Sodium-Ion Batteries. *Small* **2019**, *15*, 1805381. [CrossRef] [PubMed]
48. Dong, S.; Lv, N.; Wu, Y.; Zhang, Y.; Zhu, G.; Dong, X. Titanates for sodium-ion storage. *Nano Today* **2022**, *42*, 101349. [CrossRef]
49. Yin, J.; Zhang, Y.S.; Liang, H.; Zhang, W.; Zhu, Y. Synthesis strategies of hard carbon anodes for sodium-ion batteries. *Mater. Rep. Energy* **2024**, *4*, 100268. [CrossRef]
50. Dou, X.; Hasa, I.; Saurel, D.; Vaalma, C.; Wu, L.; Buchholz, D.; Bresser, D.; Komaba, S.; Passerini, S. Hard carbons for sodium-ion batteries: Structure, analysis, sustainability, and electrochemistry. *Mater. Today* **2019**, *23*, 87–104. [CrossRef]
51. Xiao, L.; Lu, H.; Fang, Y.; Sushko, M.L.; Cao, Y.; Ai, X.; Yang, H.; Liu, J. Low-Defect and Low-Porosity Hard Carbon with High Coulombic Efficiency and High Capacity for Practical Sodium Ion Battery Anode. *Adv. Energy Mater.* **2018**, *8*, 1703238. [CrossRef]
52. Senthil, C.; Lee, C.W. Biomass-derived biochar materials as sustainable energy sources for electrochemical energy storage devices. *Renew. Sustain. Energy Rev.* **2021**, *137*, 110464. [CrossRef]
53. Wang, J.; Zhao, J.; He, X.; Qiao, Y.; Li, L.; Chou, S.-L. Hard carbon derived from hazelnut shell with facile HCl treatment as high-initial-coulombic-efficiency anode for sodium ion batteries. *Sustain. Mater. Technol.* **2022**, *33*, e00446. [CrossRef]
54. Kamiyama, A.; Kubota, K.; Igarashi, D.; Youn, Y.; Tateyama, Y.; Ando, H.; Gotoh, K.; Komaba, S. MgO-Template Synthesis of Extremely High Capacity Hard Carbon for Na-Ion Battery. *Angew. Chem. Int. Ed.* **2021**, *60*, 5114–5120. [CrossRef]
55. Zhou, S.; Tang, Z.; Pan, Z.; Huang, Y.; Zhao, L.; Zhang, X.; Sun, D.; Tang, Y.; Dhmees, A.S.; Wang, H. Regulating closed pore structure enables significantly improved sodium storage for hard carbon pyrolyzing at relatively low temperature. *SusMat* **2022**, *2*, 357–367. [CrossRef]
56. Man, Q.; Wei, C.; Tian, K.; Shen, H.; Zhang, X.; Bai, X.; Xi, B.; Xiong, S.; Feng, J. Molecular-Level Design of High Flash Point Solvents Enables High-Safety and Dual-Function Chemical Presodiation of Hard Carbon and Alloy Anodes for High-Performance Sodium-Ion Batteries. *Adv. Energy Mater.* **2024**, *14*, 2401016. [CrossRef]
57. Rudola, A.; Rennie, A.J.R.; Heap, R.; Meysami, S.S.; Lowbridge, A.; Mazzali, F.; Sayers, R.; Wright, C.J.; Barker, J. Commercialisation of high energy density sodium-ion batteries: Faradion’s journey and outlook. *J. Mater. Chem. A* **2021**, *9*, 8279–8302. [CrossRef]
58. Schütte, M.; Laufen, H.; Luder, D.; Ditler, H.; Kern, J.; Klick, S.; Junker, M.; Stahl, G.; Frie, F.; Sauer, D.U. First full cell parameterization of a commercial layered oxide/hard carbon sodium-ion 18650 battery cell for a physico-chemical model. *J. Energy Storage* **2025**, *107*, 114931. [CrossRef]
59. Cheng, D.; Zhou, X.; Hu, H.; Li, Z.; Chen, J.; Miao, L.; Ye, X.; Zhang, H. Electrochemical storage mechanism of sodium in carbon materials: A study from soft carbon to hard carbon. *Carbon* **2021**, *182*, 758–769. [CrossRef]
60. Pendashteh, A.; Orayech, B.; Suhard, H.; Jauregui, M.; Ajuria, J.; Silván, B.; Clarke, S.; Bonilla, F.; Saurel, D. Boosting the performance of soft carbon negative electrode for high power Na-ion batteries and Li-ion capacitors through a rational strategy of structural and morphological manipulation. *Energy Storage Mater.* **2022**, *46*, 417–430. [CrossRef]
61. Web of Science. Available online: <https://www.webofscience.com/wos/woscc/summary/868023bc-3c7a-4dab-bfc3-92c8f01b13f7-0136cef274/relevance/1> (accessed on 9 January 2024).

62. Zhang, L.; Wang, W.; Lu, S.; Xiang, Y. Carbon Anode Materials: A Detailed Comparison between Na-ion and K-ion Batteries. *Adv. Energy Mater.* **2021**, *11*, 2003640. [[CrossRef](#)]
63. Tiwari, S.K.; Pandey, S.K.; Pandey, R.; Wang, N.; Bystrzejewski, M.; Mishra, Y.K.; Zhu, Y. Stone–Wales Defect in Graphene. *Small* **2023**, *19*, 2303340. [[CrossRef](#)] [[PubMed](#)]
64. Lin, Q.; Zhang, J.; Lv, W.; Ma, J.; He, Y.; Kang, F.; Yang, Q.-H. A Functionalized Carbon Surface for High-Performance Sodium-Ion Storage. *Small* **2020**, *16*, 1902603. [[CrossRef](#)]
65. Ding, J.; Wang, H.; Li, Z.; Kohandehghan, A.; Cui, K.; Xu, Z.; Zahiri, B.; Tan, X.; Lotfabad, E.M.; Olsen, B.C.; et al. Carbon Nanosheet Frameworks Derived from Peat Moss as High Performance Sodium Ion Battery Anodes. *ACS Nano* **2013**, *7*, 11004–11015. [[CrossRef](#)]
66. Wang, H.; Bai, W.; Wang, H.; Kong, D.; Xu, T.; Zhang, Z.; Zang, J.; Wang, X.; Zhang, S.; Tian, Y.; et al. 3D printed Au/rGO microlattice host for dendrite-free sodium metal anode. *Energy Storage Mater.* **2023**, *55*, 631–641. [[CrossRef](#)]
67. Wang, H.; Xu, D.; Qiu, R.; Tang, S.; Li, S.; Wang, R.; He, B.; Gong, Y.; Fan, H.J. Aligned Arrays of $\text{Na}_2\text{Ti}_3\text{O}_7$ Nanobelts and Nanowires on Carbon Nanofiber as High-Rate and Long-Cycling Anodes for Sodium-Ion Hybrid Capacitors. *Small Struct.* **2021**, *2*, 2000073. [[CrossRef](#)]
68. Costa, S.I.R.; Choi, Y.-S.; Fielding, A.J.; Naylor, A.J.; Griffin, J.M.; Sofer, Z.; Scanlon, D.O.; Tapia-Ruiz, N. Surface Engineering Strategy Using Urea to Improve the Rate Performance of $\text{Na}_2\text{Ti}_3\text{O}_7$ in Na-Ion Batteries. *Chem. Eur. J.* **2021**, *27*, 3875–3886. [[CrossRef](#)] [[PubMed](#)]
69. Zhong, W.; Tao, M.; Tang, W.; Gao, W.; Yang, T.; Zhang, Y.; Zhan, R.; Bao, S.-J.; Xu, M. MXene-derivative pompon-like $\text{Na}_2\text{Ti}_3\text{O}_7@\text{C}$ anode material for advanced sodium ion batteries. *Chem. Eng. J.* **2019**, *378*, 122209. [[CrossRef](#)]
70. Rudola, A.; Saravanan, K.; Mason, C.W.; Balaya, P. $\text{Na}_2\text{Ti}_3\text{O}_7$: An intercalation based anode for sodium-ion battery applications. *J. Mater. Chem. A* **2013**, *1*, 2653–2662. [[CrossRef](#)]
71. Tomboc, G.M.; Wang, Y.; Wang, H.; Li, J.; Lee, K. Sn-based metal oxides and sulfides anode materials for Na ion battery. *Energy Storage Mater.* **2021**, *39*, 21–44. [[CrossRef](#)]
72. Li, H.; He, Y.; Li, X.; Yu, J.; Sun, X.; Gao, T.; Zhou, G. Pomegranate-like Sn-Ni nanoalloys@N-doped carbon nanocomposites as high-performance anode materials for Li-ion and Na-ion batteries. *Appl. Surf. Sci.* **2023**, *611*, 430–462. [[CrossRef](#)]
73. Yu, D.-K.; Park, C.-M. Sb-based intermetallics and nanocomposites as stable and fast Na-ion battery anodes. *Chem. Eng. J.* **2021**, *409*, 127380. [[CrossRef](#)]
74. Pandit, B.; Sougrati, M.T.; Fraisse, B.; Monconduit, L. Exploration of a $\text{Na}_3\text{V}_2(\text{PO}_4)_3/\text{C}-\text{Pb}$ full cell Na-ion prototype. *Nano Energy* **2022**, *95*, 107010. [[CrossRef](#)]
75. Bai, Y.; Muralidharan, N.; Sun, Y.-K.; Passerini, S.; Whittingham, S.; Belharouak, I. Energy and environmental aspects in recycling lithium-ion batteries: Concept of Battery Identity Global Passport. *Mater. Today* **2020**, *41*, 304–315. [[CrossRef](#)]
76. Tang, J.; Peng, X.; Lin, T.; Huang, X.; Luo, B.; Wang, L. Confining ultrafine tin monophosphide in $\text{Ti}_3\text{C}_2\text{Tx}$ interlayers for rapid and stable sodium ion storage. *EScience* **2021**, *1*, 203–211. [[CrossRef](#)]
77. Wang, T.; Yao, K.; Hua, Y.; Shankar, E.G.; Shanthappa, R.; Yu, J.S. Rational design of MXene-MoS₂ heterostructure with rapid ion transport rate as an advanced anode for sodium-ion batteries. *Chem. Eng. J.* **2023**, *457*, 141363. [[CrossRef](#)]
78. Zhao, C.; Ding, F.; Lu, Y.; Chen, L.; Hu, Y.-S. High-Entropy Layered Oxide Cathodes for Sodium-Ion Batteries. *Angew. Chem. Int. Ed.* **2020**, *59*, 264–269. [[CrossRef](#)] [[PubMed](#)]
79. Mhaske, V.P.; Jilkar, S.; Yadav, M.D. Minireview on Layered Transition Metal Oxides Synthesis Using Coprecipitation for Sodium Ion Batteries Cathode Material: Advances and Perspectives. *Energy Fuels* **2023**, *37*, 16221–16244. [[CrossRef](#)]
80. Zhao, C.; Wang, Q.; Yao, Z.; Wang, J.; Sánchez-Lengeling, B.; Ding, F.; Qi, X.; Lu, Y.; Bai, X.; Li, B.; et al. Rational design of layered oxide materials for sodium-ion batteries. *Science* **2020**, *370*, 708–711. [[CrossRef](#)] [[PubMed](#)]
81. Guo, J.-Z.; Gu, Z.-Y.; Du, M.; Zhao, X.-X.; Wang, X.-T.; Wu, X.-L. Emerging characterization techniques for delving polyanion-type cathode materials of sodium-ion batteries. *Mater. Today* **2023**, *66*, 221–244. [[CrossRef](#)]
82. Kate, R.S.; Jadhav, H.S.; Chothe, U.P.; Bhattacharjee, K.; Kulkarni, M.V.; Deokate, R.J.; Kale, B.B.; Kalubarme, R.S. Critical review of the recent progress and challenges of polyanion $\text{Na}_3\text{V}_2(\text{PO}_4)_3$ cathode materials in rechargeable sodium-ion batteries. *J. Mater. Chem. A* **2024**, *12*, 7418–7451. [[CrossRef](#)]
83. Zhao, Y.; Gao, X.; Gao, H.; Dolocan, A.; Goodenough, J.B. Elevating Energy Density for Sodium-Ion Batteries through Multielectron Reactions. *Nano Lett.* **2021**, *21*, 2281–2287. [[CrossRef](#)]
84. Hu, P.; Zhu, T.; Cai, C.; Wang, X.; Zhang, L.; Mai, L.; Zhou, L. A High-Energy NASICON-Type $\text{Na}_{3.2}\text{MnTi}_{0.8}\text{V}_{0.2}(\text{PO}_4)_3$ Cathode Material with Reversible 3.2-Electron Redox Reaction for Sodium-Ion Batteries. *Angew. Chem. Int. Ed.* **2023**, *62*, e202219304. [[CrossRef](#)]
85. Gu, Z.-Y.; Guo, J.-Z.; Sun, Z.-H.; Zhao, X.-X.; Wang, X.-T.; Liang, H.-J.; Zhao, B.; Li, W.-H.; Pan, X.-M.; Wu, X.-L. Aliovalent-Ion-Induced Lattice Regulation Based on Charge Balance Theory: Advanced Fluorophosphate Cathode for Sodium-Ion Full Batteries. *Small* **2021**, *17*, 2102010. [[CrossRef](#)]

86. Zhuang, S.-H.; Yang, C.-C.; Zheng, M.; Rengapillai, S.; Marimuthu, S.; Chiang, Y.-S.; Chang, B.K.; Huang, C.-H.; Liu, W.-R. A combined first principles and experimental study on Al-doped $\text{Na}_3\text{V}_2(\text{PO}_4)_2\text{F}_3$ cathode for rechargeable Na batteries. *Surf. Coat. Technol.* **2022**, *434*, 128184. [CrossRef]
87. Plewa, A.; Kulka, A.; Hanc, E.; Zajac, W.; Sun, J.; Lu, L.; Molenda, J. Facile aqueous synthesis of high performance $\text{Na}_2\text{FeM}(\text{SO}_4)_3$ ($\text{M} = \text{Fe}, \text{Mn}, \text{Ni}$) alluaudites for low cost Na-ion batteries. *J. Mater. Chem. A* **2020**, *8*, 2728–2740. [CrossRef]
88. Du, G.; Tao, M.; Li, J.; Yang, T.; Gao, W.; Deng, J.; Qi, Y.; Bao, S.-J.; Xu, M. Low-Operating Temperature, High-Rate and Durable Solid-State Sodium-Ion Battery Based on Polymer Electrolyte and Prussian Blue Cathode. *Adv. Energy Mater.* **2020**, *10*, 1903351. [CrossRef]
89. Wang, C.-C.; Zhang, L.-L.; Fu, X.-Y.; Sun, H.-B.; Yang, X.-L. Hollow Layered Iron-Based Prussian Blue Cathode with Reduced Defects for High-Performance Sodium-Ion Batteries. *ACS Appl. Mater. Interfaces* **2024**, *16*, 18959–18970. [CrossRef]
90. Zhang, J.-N.; Li, Q.; Ouyang, C.; Yu, X.; Ge, M.; Huang, X.; Hu, E.; Ma, C.; Li, S.; Xiao, R.; et al. Trace doping of multiple elements enables stable battery cycling of LiCoO_2 at 4.6 V. *Nat. Energy* **2019**, *4*, 594–603. [CrossRef]
91. Altundag, S.; Altin, S.; Yaşar, S.; Altin, E. Improved performance of the NaFePO_4 /Hardcarbon sodium-ion full cell. *Vacuum* **2023**, *210*, 111853. [CrossRef]
92. Xu, J.; Zhu, S.; Xu, Z.; Zhu, H. The basic physical properties of Li_2MnO_3 and LiMn_2O_4 cathode materials. *Comput. Mater. Sci.* **2023**, *229*, 112426. [CrossRef]
93. Zhao, D.; Lu, Y.; Ma, D. Effects of Structure and Constituent of Prussian Blue Analogs on Their Application in Oxygen Evolution Reaction. *Molecules* **2020**, *25*, 2304. [CrossRef]
94. Chen, Z.-Y.; Fu, X.-Y.; Zhang, L.-L.; Yan, B.; Yang, X.-L. High-Performance Fe-Based Prussian Blue Cathode Material for Enhancing the Activity of Low-Spin Fe by Cu Doping. *ACS Appl. Mater. Interfaces* **2022**, *14*, 5506–5513. [CrossRef] [PubMed]
95. He, M.; Davis, R.; Chartouni, D.; Johnson, M.; Abplanalp, M.; Troendle, P.; Suettlerlin, R.-P. Assessment of the first commercial Prussian blue based sodium-ion battery. *J. Power Sources* **2022**, *548*, 232036. [CrossRef]
96. Bauer, A.; Song, J.; Vail, S.; Pan, W.; Barker, J.; Lu, Y. The Scale-up and Commercialization of Nonaqueous Na-Ion Battery Technologies. *Adv. Energy Mater.* **2018**, *8*, 1702869. [CrossRef]
97. Kuan, H.-C.; Luu, N.T.H.; Ivanov, A.S.; Chen, T.-H.; Popovs, I.; Lee, J.-C.; Kaveevivitchai, W. A nitrogen- and carbonyl-rich conjugated small-molecule organic cathode for high-performance sodium-ion batteries. *J. Mater. Chem. A* **2022**, *10*, 16249–16257. [CrossRef]
98. Wang, L.; Liu, N.; Zhao, X.; Wang, X.; Zhang, T.; Luo, Z.; Li, F. Copper and conjugated carbonyls of metal-organic polymers as dual redox centers for Na storage. *Chem. Sci.* **2024**, *15*, 2133–2140. [CrossRef] [PubMed]
99. Du, K.; Wang, C.; Subasinghe, L.U.; Gajella, S.R.; Law, M.; Rudola, A.; Balaya, P. A comprehensive study on the electrolyte, anode and cathode for developing commercial type non-flammable sodium-ion battery. *Energy Storage Mater.* **2020**, *29*, 287–299. [CrossRef]
100. Rong, J.-Z.; Cai, T.-X.; Bai, Y.-Z.; Zhao, X.; Wu, T.; Wu, Y.-K.; Zhao, W.; Dong, W.-J.; Xu, S.-M.; Chen, J.; et al. A free-sealed high-voltage aqueous polymeric sodium battery enabling operation at -25°C . *Cell Rep. Phys. Sci.* **2022**, *3*, 100805. [CrossRef]
101. Janakiraman, S.; Khalifa, M.; Biswal, R.; Ghosh, S.; Anandhan, S.; Venimadhav, A. High performance electrospun nanofiber coated polypropylene membrane as a separator for sodium ion batteries. *J. Power Sources* **2020**, *460*, 228060. [CrossRef]
102. Zhang, L.; Li, X.; Yang, M.; Chen, W. High-safety separators for lithium-ion batteries and sodium-ion batteries: Advances and perspective. *Energy Storage Mater.* **2021**, *41*, 522–545. [CrossRef]
103. Liu, H.; Zheng, X.; Du, Y.; Borrás, M.C.; Wu, K.; Konstantinov, K.; Pang, W.K.; Chou, S.; Liu, H.; Dou, S.; et al. Multifunctional Separator Enables High-Performance Sodium Metal Batteries in Carbonate-Based Electrolytes. *Adv. Mater.* **2024**, *36*, 2307645. [CrossRef]
104. Song, Y.; Sheng, L.; Wang, L.; Xu, H.; He, X. From separator to membrane: Separators can function more in lithium ion batteries. *Electrochim. Commun.* **2021**, *124*, 106948. [CrossRef]
105. Zhou, D.; Tang, X.; Guo, X.; Li, P.; Shanmukaraj, D.; Liu, H.; Gao, X.; Wang, Y.; Rojo, T.; Armand, M.; et al. Polyolefin-Based Janus Separator for Rechargeable Sodium Batteries. *Angew. Chem. Int. Ed.* **2020**, *59*, 16725–16734. [CrossRef]
106. Muddasar, M.; Beaucamp, A.; Culebras, M.; Collins, M.N. Cellulose: Characteristics and applications for rechargeable batteries. *Int. J. Biol. Macromol.* **2022**, *219*, 788–803. [CrossRef] [PubMed]
107. Saltwater Battery: The Safest Long-Term Storage Solution. Available online: <https://www.aquionenergy.com/technology/aqueous-hybrid-ion-ahi/> (accessed on 9 January 2024).
108. Li, R.-R.; Yang, Z.; He, X.-X.; Liu, X.-H.; Zhang, H.; Gao, Y.; Qiao, Y.; Li, L.; Chou, S.-L. Binders for sodium-ion batteries: Progress, challenges and strategies. *Chem. Commun.* **2021**, *57*, 12406–12416. [CrossRef] [PubMed]
109. Larsson, F.; Andersson, P.; Blomqvist, P.; Mellander, B.-E. Toxic fluoride gas emissions from lithium-ion battery fires. *Sci. Rep.* **2017**, *7*, 10018. [CrossRef]